STRAIN INDUCED ENERGY BAND-GAP OPENING OF SILICENE

A thesis submitted in partial fulfillment of the requirements for the degree of Master of Science in Engineering

By

Zhonghang Ji

B.S.E. Changchun Institute of Technology, 2011

2015

Wright State University

WRIGHT STATE UNIVERSITY

GRADUATE SCHOOL

May 19, 2015

I HEREBY RECOMMEND THAT THE THESIS PREPARED UNDER MY SUPERVISION BY Zhonghang Ji, ENTITLED Strain induced energy band-gap opening of silicene BE ACCEPTED IN PARTIAL FULFILLMENT OF THE REQUIREMENTS FOR DEGREE OF Master of Science in Engineering.

Yan Zhuang, PH.D.

Thesis Director

Brian Rigling, PH.D. Chair

Department of Electrical Engineering

Committee on

Final Examination

Yan Zhuang, PH.D.

Lok C. Lew Yan Voon, PH.D.

Marian K. Kazimierczuk, PH.D.

Robert E.W. Fyffe, PH.D.

Vice President for Research and

Dean of Graduate School

Abstract

Ji, Zhonghang. M.S.Egr. Department of Electrical Engineering, Wright State University, 2015. Strain-induced energy band-gap opening of silicene.

Inspired by the success of graphene, various two dimensional (2D) structures on different substrates have been proposed. Among others, an allotropic form of silicon, coined “silicene” was shown to exhibit similar properties with graphene of a zero band gap and a Dirac cone shape at the K point in the Brillouin zone. Similar to its counterpart graphene, one of the main obstacles to applying silicene in modern electronics is the lack of an energy band gap. In this work, a systematic study was presented on the structural and electronic properties of single and bi-layered silicon films under various in-plane biaxial strains. The modeling was performed using density functional theory. The atomic structure of the 2D silicon films was optimized and verified by using both the local-density approximations and generalized gradient approximations. Energy band diagram, electron transmission efficiency, and the charge transport property were calculated. It turns out that single free-standing 2D silicon film, i.e. silicene, does not present any energy band gap opening under biaxial tensile/compressive in-plane strain/stress, while bi-layered silicon film exhibits an energy band gap as the applied in-plane tensile strain reaches above 10.7%. In

addition, the energy band gap of the bi-layered silicon film shows a linear dependency on the applied in-plane strain and reaches a maximum of about 168.0 meV as the in-plane tensile strain reaches ~ 14.3%. Single and bi-layered silicon films grown on various common semiconductor substrates have been modeled. By choosing the proper substrate, an energy band gap can be opened for the bi-layered silicon film. This will provide an opportunity for applying 2D silicon structure in the mainstream IC industry.

Contents

List of Figures

Acknowledgements

First and foremost I would like to thank my advisor, Dr. Yan Zhuang, who was so much than an advisor; he was a friend, a mentor, a teacher. Thanks him for the continuous support of my Master study and research. A lot of patience, motivation, enthusiasm, immense knowledge was shown by him on helping me in all the time of research and writing of this thesis. Without his help and guidance, this thesis would not have been possible.

Secondly, I would like to thank Dr. Lok. C. Lew Yan Voon for his help and encouragement. I really learned a lot from your suggestions and guidance. Your support, time and energy are greatly appreciated. I could not have finished without you.

The simulation of this work has been rough at times, and I have to thank to Anders Blom, who helped me solving lots of technique issues.

Lastly, I want to thanks my parents and my wife for their unselfish support.

Chapter 1 Introduction

1.1 Background of research

It is well-known the semiconductor industry has been playing a significant role in our daily life. The rapid development is attracting more and more researchers to devote themselves to this field. Presently, the integrated circuits (ICs) occupy the majority of the semiconductor market. They are widely used in virtually all electronics today and are becoming indispensable components to our life, such as cell phones, computers, and other digital applications due to the low cost and the high performance.

Nowadays, silicon is the most popular material used in the ICs for decades. In order to increase the processing speed and optimize the performance, up to trillions of transistors are integrated on a single chip. This means the size of the transistors is dramatically reduced. However, as silicon is reaching its physical limitation, the short channel effect becomes formidable. Up to date, several approaches are under investigations, and some of them have already been applied in industry. For example, high-k materials have been used to replace the silicon-dioxide gate oxide layer used to increase gate capacitance and to allow continued transistor scaling down. Another one is silicon on insulator (SOI) technology which was announced by IBM in August

1988. This technology can reduce the short channel effect by reducing parasitic device capacitance.

The appearance of graphene attracted more researchers' attention. Due to its high electron mobility and the single atomic layer feature, graphene can be potentially used as the channel layer in the field-effect transistor to further increase the speed. Graphene based transistor has been demonstrated with record cutoff frequency up to 300GHz [1]. The major bottleneck preventing graphene from the mainstream semiconductor industry is the lack of an energy band gap. There are tremendous efforts to develop graphene with energy band gap including doping, nanoribbon [2], … However, there is no reliable method to induce an energy band gap into graphene. Therefore, attempts to look for other two dimensional (2D) materials have been taken into account. Among all the other 2D materials, such as MoS2, germancene, Borophene, and Phosphorene, silicene shows the most promising characteristic because it is fully compatible with the silicon technology. Similar to its counterpart graphene, silicene also suffers from the lack of an energy band gap. An important research project is to develop the technology required to induce an energy band gap into silicene.

1.2 Review of Graphene

Graphene is a single layer of carbon atoms arranged in a honeycomb lattice which shown in Figure 1.1. Technically, graphene is a crystalline allotrope of carbon with two-dimensional materials' properties. The carbon atoms form sp^2 bonds which look like chicken wire the so-called hexagonal structure. At first, graphene was used to describe a single sheet of graphite as a constituent of graphite intercalation compounds (GICs) in 1987[3]. Actually, starting from the 1970s, single layer graphene was obtained by growing epitaxially on specified substrates. Nevertheless, the thickness could not be thinner than 50 layers until 2004. In 2004, Andre Geim and Kostya Novoselov at the University of Manchester, extracted single-atom-thick crystallites from bulk graphite, for which they were awarded with Nobel Prize in Physics in 2010 [4]. The way they got the graphene was to peel off a few layers from graphite until only one layer remained. Although graphene can be obtained by using other methods like epitaxy, chemical vapor deposition, and supersonic spray, mechanical exfoliation is still the most effective method to obtain high performance graphene.

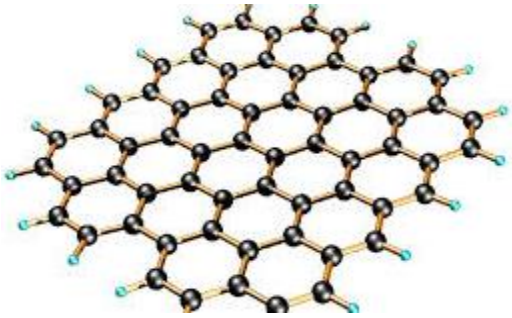

Figure 1.1 Atomic structure of graphene arranged in a honeycomb lattice.

Graphene shows the hexagonal structure, the distance between the nearest 2 carbon atoms is 0.14nm. Extensive studies of the structural properties of graphene have been carried out using transmission electron microscopy (TEM), scanning tunneling microscopy (STM), and atomic force microscopy (AFM) (Fig. 1.2).

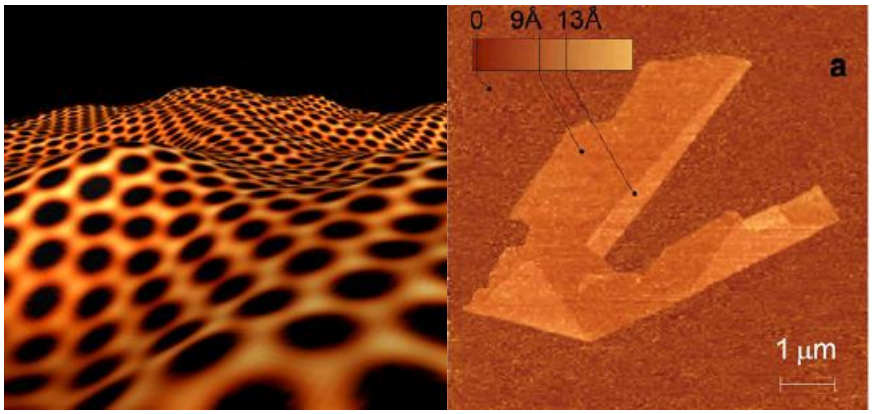

Figure 1.2 STM (a) and AFM (b) - microscopic images of graphene [5].

Graphene exhibits excellent electronic, thermal, and mechanical properties [6], at room temperature, the record-high electron mobility is reported beyond 100,000 $cm^2*V^{-1}*S^{-1}$[7]. The thermal conductivity reaches up to 2500 $W \cdot m^{-1} \cdot K^{-1}$ [8]. The

mechanical strength of graphene was reported to be the strongest [9]. The Dirac cone shaped energy band diagram (Fig. 1.3) allows applications of graphene into high speed electronics and optoelectronics.

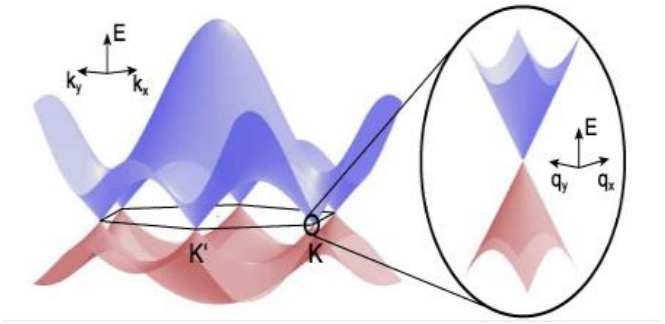

Figure 1.3 Electronic dispersion of graphene and zoom in the dispersion [10].

Although the properties of graphene are excellent and a number of graphene-related devices have been demonstrated, building graphene based FETs is still presenting a big challenge. The lack of a band gap makes the graphene based transistor difficult to be switched off. Therefore, people started looking for other graphene-like materials which can be used in modern electronics.

1.3Review of Silicene

Silicene, a graphene-like 2-dimentional silicon, has a honeycomb lattice. In 1994, first principels total energy calculation was employed to investigate the silicon-based

nanosheets[11]. Then in 2007, silicene was studied using a tight-binding Hamiltonian by [12]. The hexagonal structure of silicene is showed in Figure 1.4. Unlike graphene, the basal plane of the silicene is not flat because the electrons of silicon atoms try to form the tetrahedral sp^3 hybridization and the buckle structure seems to be more stable than the flat one [13].

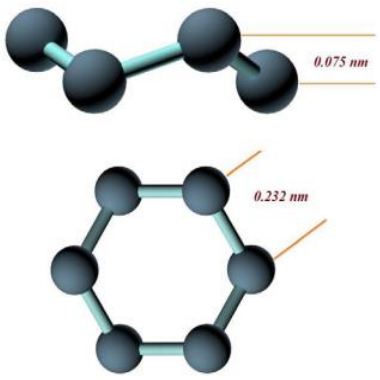

Figure 1.4 Hexagonal structure of silicene [14].

Compared to graphene, silicene is difficult to be obtained experimentally. Mechanical exfoliation of silicene from bulk silicon is impossible due to the covalent Si-Si bonds [15]. The first reported observation of silicene was obtained in 2010 by using scanning tunneling microscope [16]. In their studies, silicene film was deposited using atomic resolution and silver was used as the substrate. This result (Fig. 1.5) shows the honeycomb arrangement of silicene, though the result is being disputed. In 2012,

several groups independently reported ordered phases on the Ag (111) surface [17].

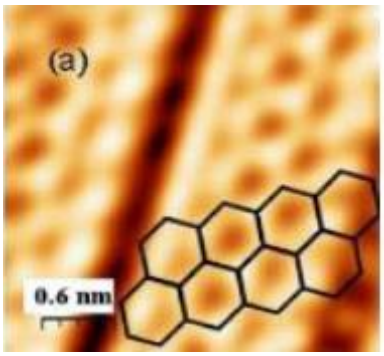

Figure 1.5 Honeycomb arrangement of Silicene [16]

Silicene shows different electrical properties from graphene. For instance, by applying an external voltage, the tunable band gap in silicene can be obtained (Fig. 1.6) [18]. Also, to third order in the wave vector, silicene exhibits anisotropy in the band structure while it occurs at the quadratic order for graphene [19]. Potential applications of silicene were found in electronic, thermoelectric, photovoltaic, optoelectronic, and spintronic devices [20]. In this thesis, research is mainly focused on applying silicene in electronic devices. Compared to graphene, silicene is friendlier with the existing silicon technology.

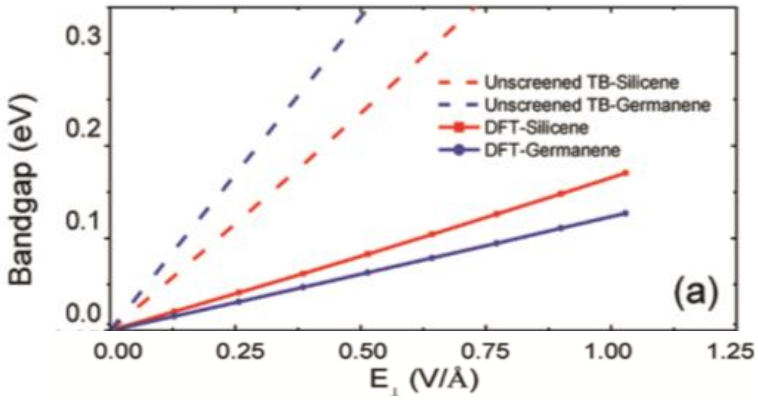

Figure 1.6 band gap of silicene and germanene obtained by applying different vertical electric field. Dot lines denote TB mode land solid lines denote DFT model.

1.4Band gap-opening in 2D materials

The properties of 2D materials have been attracting more and more attention since graphene was discovered in 2004. However, the lack of a band gap is still the biggest challenge. To circumvent it, more effort was paid to find a band gap in other types of 2D materials. Some studies have reported that MoS_2 have a large intrinsic band gap of 1.8 eV. However, the mobility of the single layers is 0.5-3$cm^2V^{-1}s^{-1}$ and is too low for practical devices [21]. In 2011, another group demonstrated a single-layer MoS_2 whose mobility can reach 200$cm^2V^{-1}s^{-1}$ at room temperature by using a hafnium oxide gate dielectric [22]. Even though MoS_2 has a band gap, its low mobility prevents it

from transistor applications. For this reason, numerous theoretical attempts for silicene including chemical functionalization, formation of nanoribbons, applying external electrical field, and intentional generation of lattice imperfection have been tried to open the energy band gap while preserving the integrity of the silicene's honeycomb atomic structure [23-38]. Integration of chemically functionalized silicene into the standard silicon processing imposes a formidable challenge since many processes are carried out at high temperature like the formation of gate oxide and exposed in various chemicals (e.g. plasma etching). Energy band gap opened in silicene nanoribbons strongly depends on the width of the nanoribbons. Any tiny variation of the width caused by the processing tolerance will lead to significant change of the energy band gap and consequently the device performance. Applying external electrical field to open the band gap indicates more energy consumption, while inducing defects in silicene will significantly deteriorate the device performance and reduce its life time. Experimentally, silicene has been demonstrated on a variety of metallic substrates, such as silver (Ag) [27-33](9-15), zirconium diboride (ZrB2)[34](16), gold (Au)[39](zy31), and iridium (Ir)[35](17). However, the preferred substrates for integrated FET devices are group IV, III-V, and II-VI semiconductor substrates.

1.5 Strain in 3D bulk semiconductor materials

Deformation in general consists of elastic, plastic and viscous deformation. Strain engineering has been applied to modify the energy band diagram of semiconductor materials since 1951 by Hall. [40]. In 1954, Smith studied the effect of strain on the conductivity of Si [41]. To avoid defects generation, the level of strain is constrained in the elastic range. In his work, the resistivity of silicon changed dramatically by applying a uniaxial tensile strain, which is due to the change of the energy band diagram. Basically, the induced strain breaks the symmetry of the original structure and leads to a shift in the energy levels of conduction and valence bands. This principle was first time applied to build an n-type metal-oxide-field-effect-transistor (nMOSFET) by J. Welser and J. Hoyt [42]. The results show a 70% higher effective mobility than those with unstrained Si. The p-channel MOSFETs work which is related to mobility enhancement by biaxial stress was demonstrated by Oberhuber and Fischetti, in their work, both compressive and tensile strain are found to enhance the mobility, while confinement effects result in a reduced hole mobility for a Si thickness ranging from 30 to 3 nm [43].

1.6 Scope of current research

In this work, a systematic study is presented on the structural and electronic properties

of single and bi-layered silicon films under various in-plane biaxial strains. The modeling was performed using density functional theory. The atomic structure of the 2D silicon films was optimized and verified by taking into account both the local-density approximations (LDA) and generalized gradient approximations (GGA). Energy band diagram, electron transmission efficiency, and the charge transport property were calculated. By inducing the proper strain, an energy band gap in a bi-layered silicon film can be opened. This will provide an opportunity to apply 2D silicon structures in the mainstream IC industry.

Chapter 1: Introduction of properties of graphene and silicene, and strain induced on 3D semiconductor materials.

Chapter 2: Introduction on calculation method DFT and software ATK, and verification on graphene.

Chapter 3: Energy band diagrams of strained single and bi-layered silicon layer.

Chapter 4: The Selection of substrate and the analysis of experimental results.

Chapter 2 DFT model of 2D material

Density functional theory (DFT) is a computational quantum mechanical atomistic modeling method. It has been widely used in modeling of the electronic structure focusing on atoms, molecules, and the condensed phases. Local-density approximations (LDA) and generalized gradient approximations (GGA) are the two main approximations by taking approximations to the exchange-correlation potential and taking approximation of the local gradient of the density, respectively. In present work, both LDA and GGA are employed to calculate the energy band structure, transmission spectrum, I-V curve, and density of state.

The DFT calculations were performed using Atomistix Tool-Kit (ATK) provided by QuantumWise, which is a multi-purpose atomic-scale modeling platform. ATK allows atomic-scale computations on electronic structure, energy band diagram, and charge transport. Over 300 LDA/GGA exchange-correlation approximations are included. In addition, van der Waals force has been included in the computation model (DFT D2).

To verify the validity of the ATK-DFT model, graphene has been chosen as an example. During the calculation, both the local density approximation (LDA) and the generalized gradient approximation (GGA) are employed to optimize the atomic

structure based on the DFT theory. The LDA gives a slightly smaller lattice constant then GGA due to the different approximation. Both results perfectly match to other reported work [4][10]. In our work, all calculations are computed by using GGA, which is more accurate than LDA in most cases. In order to minimize the impact from the adjacent carbon layers in a supercell calculation, the lattice constant along the out of plane i.e. z-axis was set to 20 Å, which can reduce the effect of interlayer coupling. A 21×21×1 Monkhorst-Pack grid k-point mesh has been used along the x-, y-, and z-axis for the Brillouin zone sampling. Usually, during the calculation, the more points employed, the more accurate results will get, and also the longer time will be taken. In addition, the force tolerance, density mesh cut-off and electron temperature were set at the value of 0.001 eV/Å, 75 Hartree and 300K, respectively. The force tolerance is used to find the minimum energy point during the simulation. Since the force tolerance is the derivative of energy to distance, lowering the force tolerance will get more stable structure. The mesh cut-off is an energy which corresponds to the fineness of the real-space grid on which the Poisson equation is solved. Usually, the higher value of the mesh cut-off set, the better real-space grid and accuracy will get. For the electron temperature, actually, the temperature will have effect on calculating transmission spectrum. If the temperature increases, the range of occupied states will be broadened. Then the system will generate hot electrons that can easily cross a

potential barrier which is called thermionic emission. As a result, the electron temperature usually is set to 300K. Periodic boundary condition has been employed for unit cells 1×1, 2×2, and 3×3 (show in Figure 2.1).

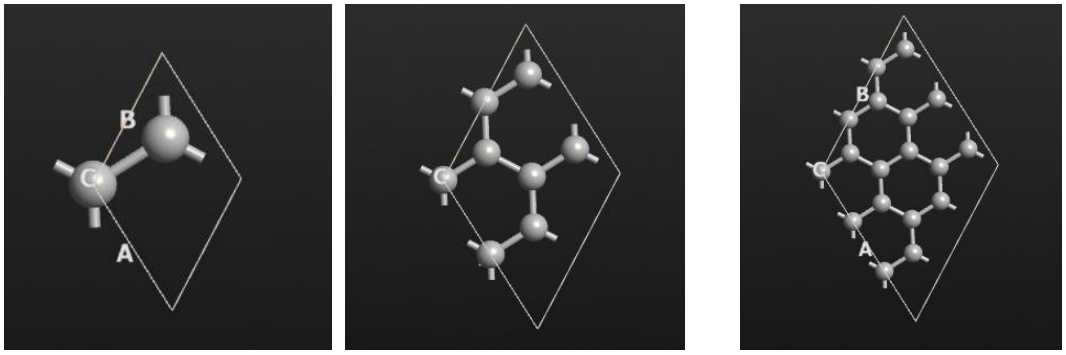

A B C

Figure 2.1 Atomic structure of 1×1 (A), 2×2(B), and 3×3(C) of graphene.

After optimization, the atomic structure shows 0 Å buckling height and hexagonal structure shown in Figure 2.2. The band diagram is showing in Figure 2.3. The bond length equals to 1.42 Å and the lattice constant is 2.4612 Å. In addition, perturbation is added to verify the structure's stability.

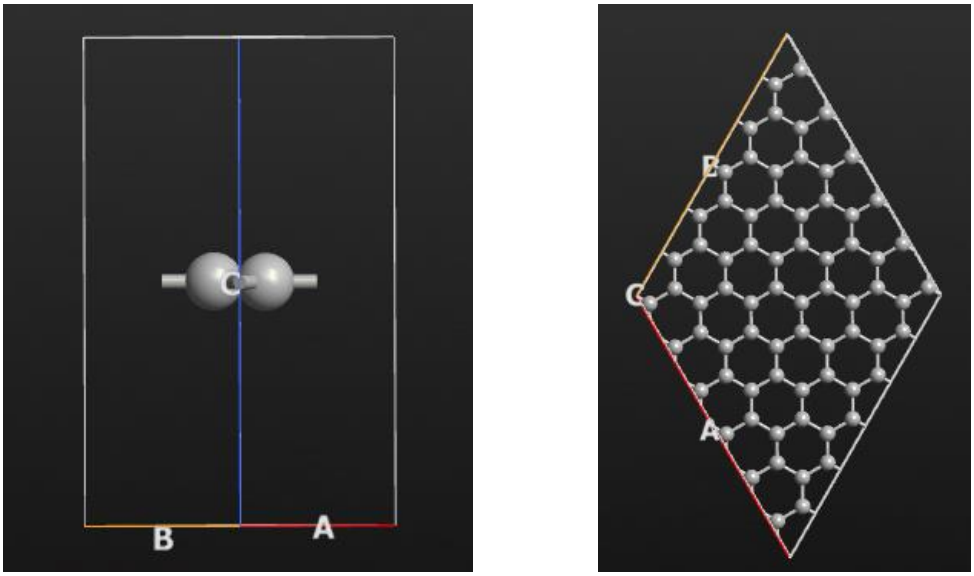

Figure 2.2 Optimized graphene side view (left) and top view(right) of duplicated 9×9 structure

The excellent agreement between our simulations and published results validates the atomic model of graphene (Rignanese & Charlier). The transport properties were calculated by solving the non-equilibrium Green's function (NEGF) with norm-conserving pseudo-potentials. The Dirac cone is clearly observed at the K-point. There is no band gap. Due to this reason, the transmission efficiency at Fermi energy level equals to zero which shows in Figure 2.4. I-V curve shows in Figure 2.5.

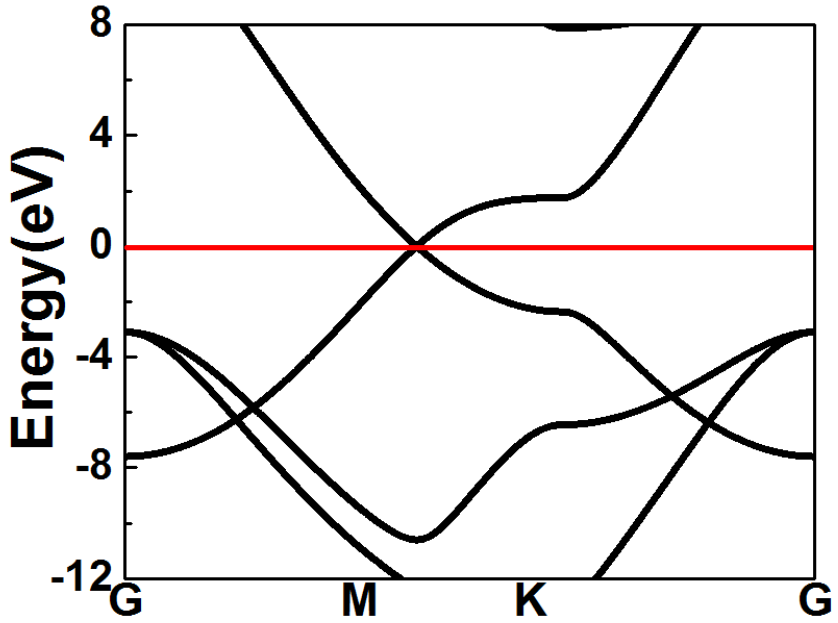

Figure 2.3 Band diagram of graphene. Dirac cone shows at K point.

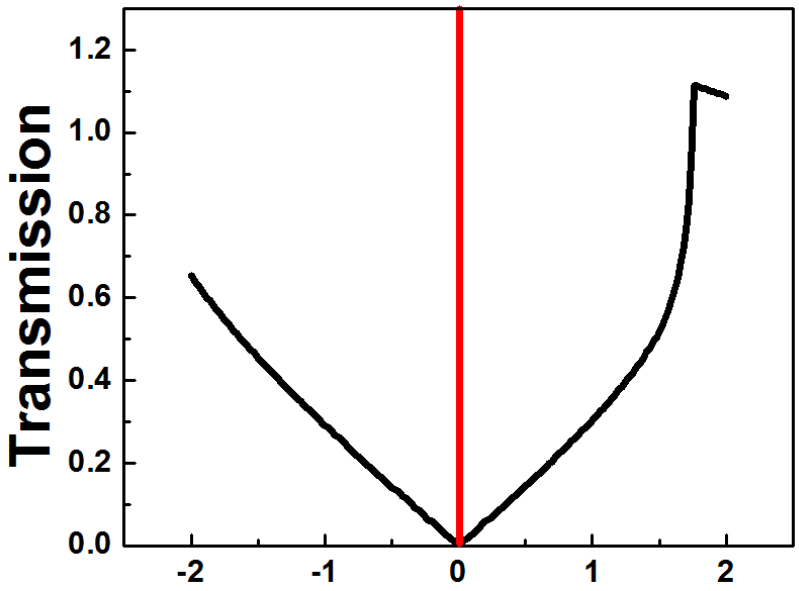

Figure 2.4 Transmission spectrum of graphene. At Fermi energy level, the transmission efficiency is aero.

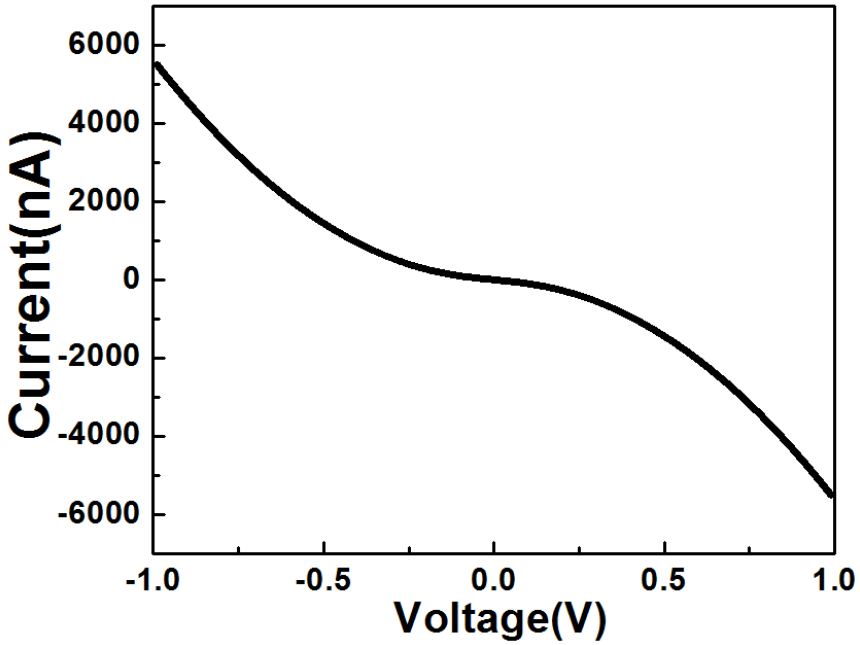

Figure 2.5 I-V curve of graphene. The current is continually decreases from -1V to 1V due to the gaplessness of graphene.

Chapter 3 Energy band diagrams of strained single and bi-layered silicon layer

3.1 Introduction

Even though graphene has extremely charming properties and can be applied in different kinds of fields, however, the gapless problem is still the biggest challenge to be applied on FET in electronic field. Silicene also has very promising properties. Up to now, numerous experiments have been already performed based on silicene and its derivatives as mentioned in chapter 1 and chapter 2. Since silicene has an advantage that it can be compatible perfectly with current Si technique compared with graphene, trying to find a band gap based on silicene and its derivatives is significantly important.

3.2 Single silicon layer

Strain engineering has been widely applied in Si technology to enhance the high frequency performance such as current drive and cut-off frequency [44]. It can be instrumental in improving electron and hole mobility by inducing either compressed or tensile strain/stress. However, few works addressed the impacts of strain/stress on

the energy band diagram of 2-D materials. It is anticipated that the energy band diagram can be significantly modified [45] due to silicene's single atomic layer feature. It has been reported that the properties of silicene showed considerable change with strain above 7% [6]. Nevertheless, these structures do not exhibit any band gaps, limiting their applications in the mainstream semiconductor industry. In this work, I performed DFT calculations to explore the feasibility of band gap opening in freestanding relaxed and strained single and bi-layered silicon film.

3.2.1 Free standing single silicon layer

Computation of free standing single silicon layer based on DFT theory, i.e. silicene, has been performed to verify the model and the results are compared with the numbers in the published work. The atomic structure has been optimized using GGA. In order to minimize the impact from the adjacent silicon layers, the lattice constant along the out of plane i.e. z-axis was set to 25 Å, which means there is at least 10 Å vacuum between two layers in the z direction. A 21×21×1 Monkhorst-Pack grid k-point mesh has been used along the x-, y-, and z- axis for the Brillouin zone sampling. In all the calculations, the force and stress tolerance, density mesh cut-off and electron temperature were set at the value of 0.0001 eV/Å, 75 Hartree and 300K, respectively. Also the non-polarized correlation was added to the calculation. The

Si-Si bond length is 2.342 Å. Periodic boundary condition has been employed for unit cells 1×1, 2×2, and 3×3 to optimize the atomic structure. The excellent agreement between our simulations and the published results validates the atomic model of single layer silicon. The transport properties were calculated by using FFT in solving the non-equilibrium Green's function (NEGF) with norm-conserving pseudo-potentials.

Figure 3.1 shows the optimized atomic structure of a single free standing silicon layer. Similar as reported in [12][46], single layer silicon forms a 2-D honeycomb structure (silicene) with an in-plane lattice constant 3.866 Å and a buckling height of 0.5099 Å using GGA approximation. The atomic structure has been verified by choosing various unit cells 1×1, 2×2, and 3×3, and the results show excellent agreement. LDA approximation and molecular dynamic simulations have been carried out for further verification of the structure, the lattice constant is little smaller than the one obtained from GGA, and the buckling distance is 0.51 Å which has 0.0001 difference with GGA's result, and all the results show good agreement with reported work. Based on the model used, a large variation of lattice constant of silicene exists in the literature [47][48], ranging from 3.83 Å to 3.88 Å. A range of buckling height (0.42 Å to 0.53 Å) have been reported by a number of groups [49][50]. Both the lattice constant and the buckle height obtained in our work are in good agreement with the published results,

verifying the validity of our model. The calculated band diagram of silicene is shown in figure 3.2. Similar to the work of Guzman-Verri and Lew Yan Voon, silicene shows a Dirac-cone shape near the K-point with zero band gap. The transmission spectrum and the I-V curves are shown in Figs. 3.3 and 3.4. the numerical errors in our simulations lead to the tiny kink on the I-V curve near zero voltage.

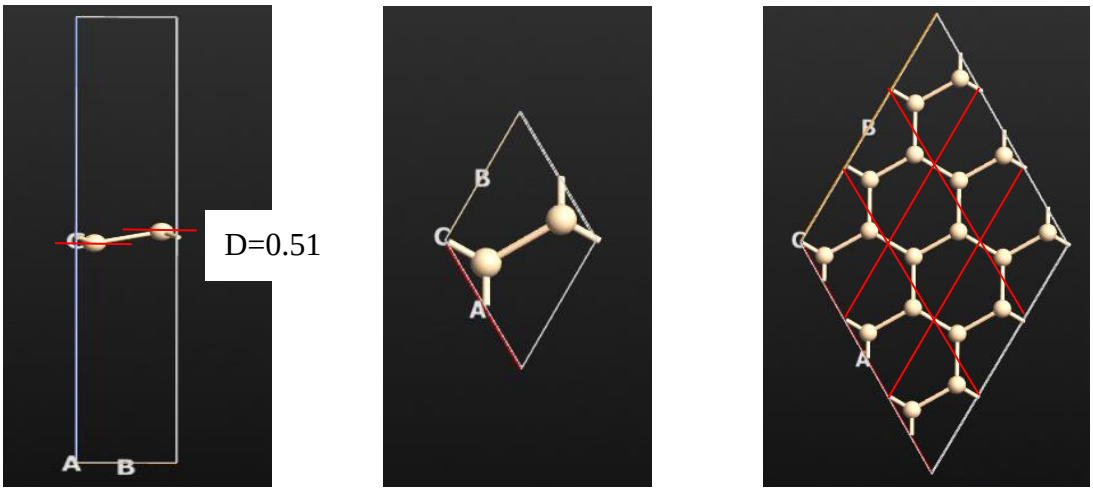

α β γ

Figure 3.1 α) Side view of silicene. β) Top view of 1 by 1 silicene. γ) Top view of 3 by 3 silicene,

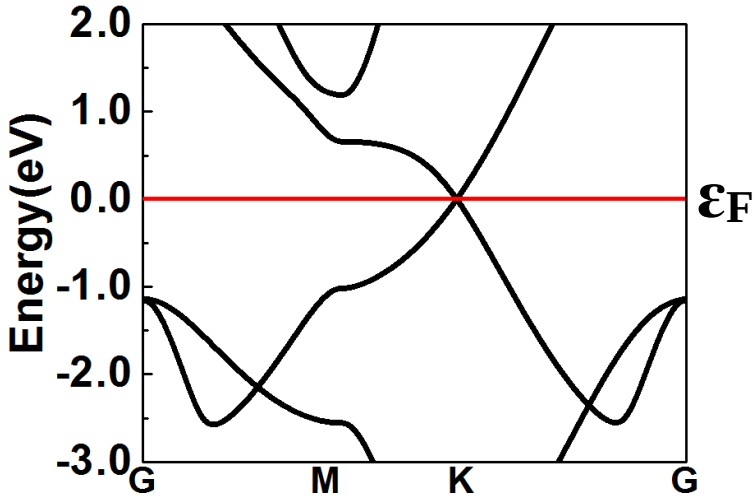

Figure 3.2 Band diagram of silicene. Dirac point is in line with the Fermi energy level.

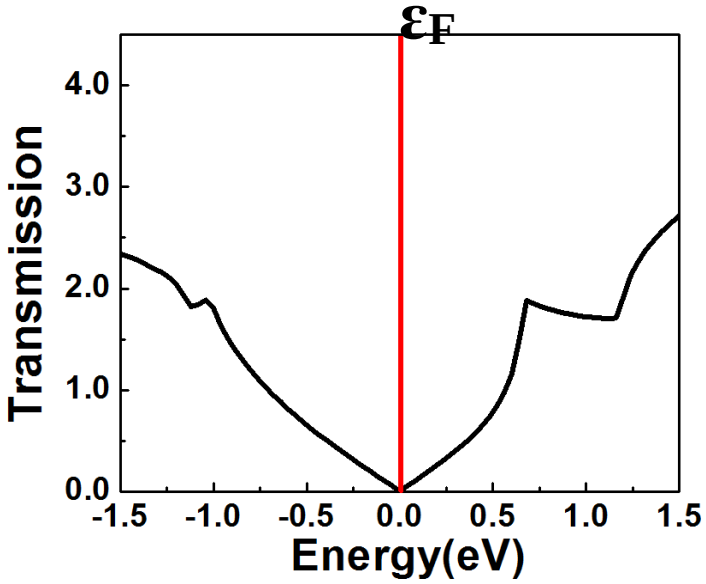

Figure 3.3 Transmission spectrum of silicene.

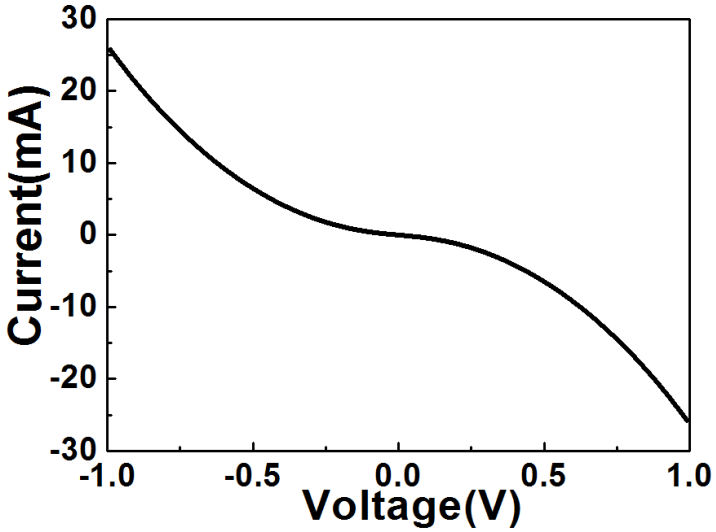

Figure 3.4 The I-V curve of silicene.

3.2.2 Biaxial strained single silicon layer

The atomic structure of a single layer silicon under either tensile or compressive strain has been computed and optimized using DFT with the same setting parameters as those for the free standing silicon layer. The electrical transport properties including energy band diagram and transmission spectrum have been calculated and compared to the various induced strain. The initial values of Si-Si bond length and the relative positions of the two silicon atoms are chosen as the same as the free standing silicon layer. The strain is induced by modifying the lattice constant, i.e. tensile strain from 3.866 Å up to 4.366 Å (about 12.9%), and compressive strain from 3.866 Å down to 3.566 Å (about 7.8%). The strain is applied in the 2-D lattice plane.

The results of the buckling height of the silicene versus induced strain is plotted in

figure 3.5 and listed in table 1. In general, the buckling height monotonically decreases by enlarging the lattice constant of silicene, but showing different characteristics in tensile- and compressive- strain regions. Increasing of lattice constant in the compressive strain region, i.e. reducing the compressive strain, leads to a linear decrease of the buckling height. The buckling height reaches the maximum value 0.796 Å when the lattice constant equals to 3.566 Å, showing a ~56.1% increase compare to the free-strain reference. However, the buckling height exhibits a weak dependency (0.415 Å ~ 0.421Å) upon further increasing of the lattice constant in the tensile-strain region.

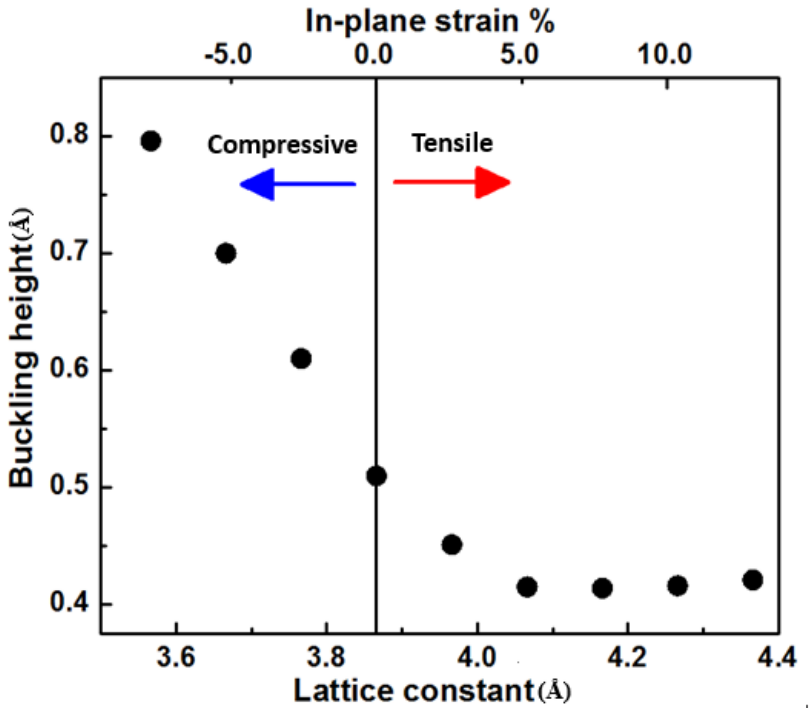

Figure 3.5 Buckling height of the silicene versus induced strain. The left region shows the buckling height with different compressive strain. The right region shows the buckling height with different tensile strain.

Dependency of Si-Si bond length on the induced strain is shown in figure 3.6. The bond length monotonically increases with the lattice constant. Compared to figure 3.5, the tensile-strain tends to form a “flat” structure with a smaller buckling height by elongating the Si-Si bond length. The compressive-strain tends to form a structure with larger buckling height and at the same time shortens the bond length.

Table 1

Lattice constant (Å)	Buckling distance(Å)	Bond length(Å)	Strain %
3.566	0.796	2.205	7.76
3.666	0.7	2.227	5.17
3.766	0.61	2.258	2.59
3.866	0.51	2.288	0
3.966	0.451	2.336	2.59
4.066	0.415	2.384	5.17
4.166	0.414	2.437	7.76
4.266	0.416	2.494	10.3
4.366	0.421	2.563	12.9

Other groups also did similar work based on biaxially strained silicene. A 0.34 Å buckling height was obtained with a 12.5% strain by Liu et al. [51]. Another group

also reported that a stable flat silicene was obtained by inducing a 20% strain. [52]. However, this disagrees with other groups. There are two groups which also found that the buckling height reduced to 0.3 Å with 10% strain and 0.23 Å with 7% strain.[53][54]. Our result is a little higher than theirs.

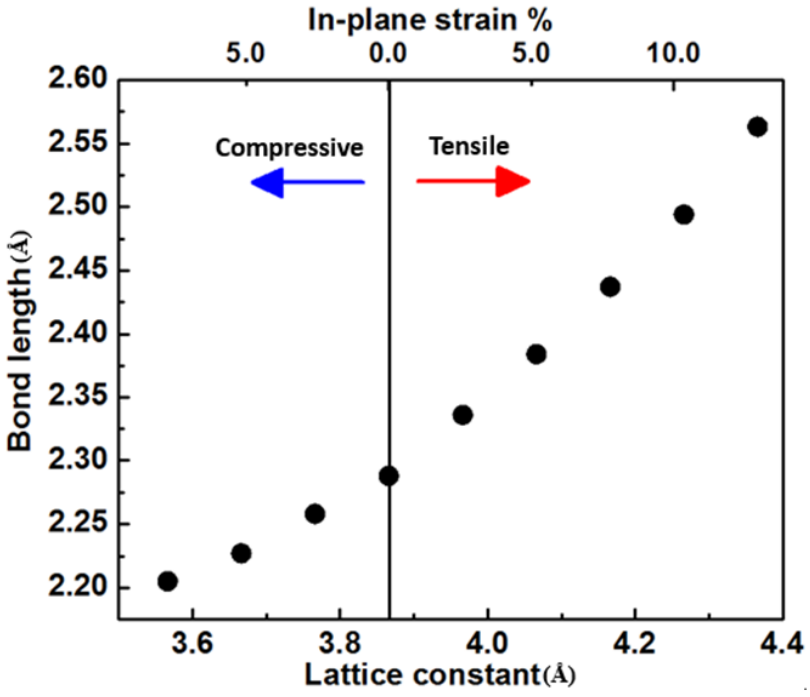

Figure 3.6 Si-Si bond length on the induced strain. The left region shows the bond length with different compressive strain. The right region shows the bond length with different tensile strain.

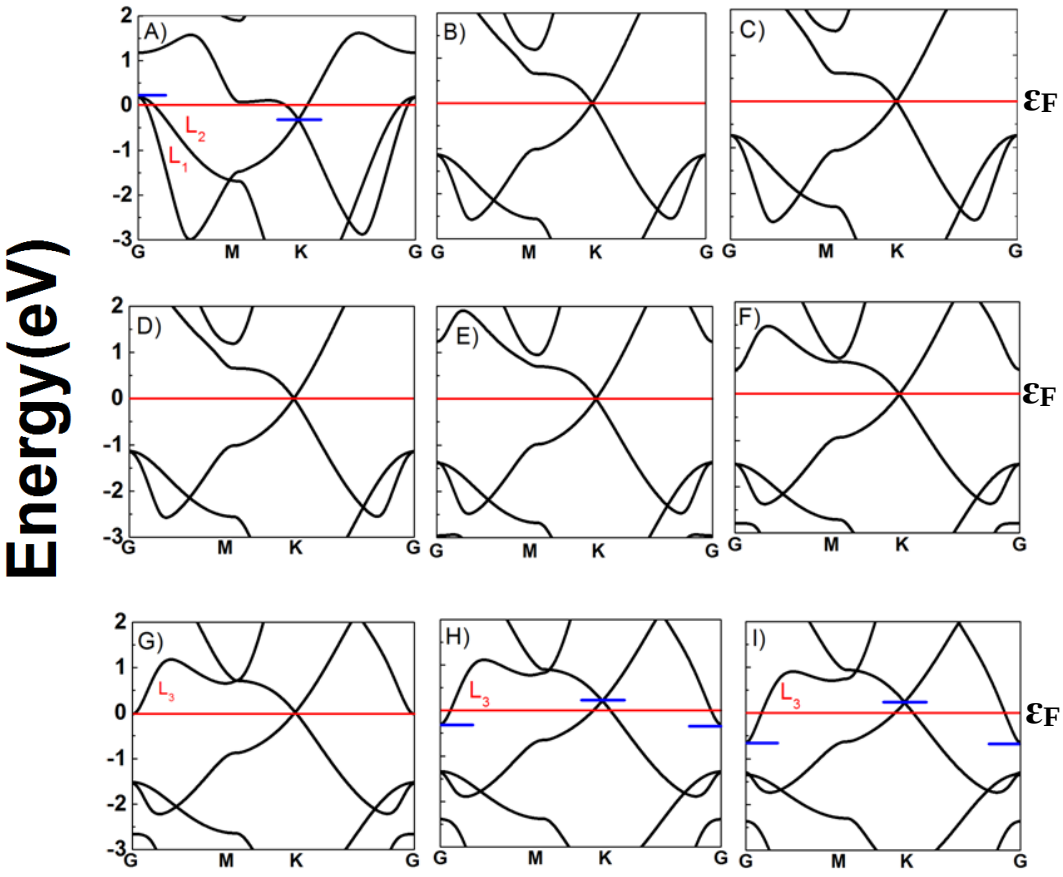

Figure 3.7 A – I show band diagrams by giving the lattice constant from 3.566 Å from 4.366 Å. Fermi energy level is denoted with the red line. The blue lines show the energy offset of Dirac point, energy bands L1 and L2 in (A), and L3 in (H) and (I). Figures (B)-(F) show features of direct semiconductor materials, while figures (A), and (G)-(I) show features of indirect semiconductor materials due to the crossing of energy bands L1, L2, and L3 with the Fermi energy level.

Figure 3.7 shows the band diagrams of silicene by giving different compressive and tensile strain. Dirac cone is observed in all the band diagrams. When the lattice constant equals to the reference value 3.866 Å, the silicene structure shows the feature of a direct semiconductor material with the Dirac cone coincident with the Fermi energy level at the K-point. As the induced compressive strain is small (Figs. 3.7 B and C), there is no noticeable shift of the Fermi energy level. Further enlarging the compressive strain (Fig. 3.7 A), the silicene structure shows the feature of an indirect semiconductor material. The energy bands L_1 and L_2 rise above the Fermi energy level and exhibit a maximum at the G-point. Contrary to the compressive strain, a tensile strain leads to a lowering of the Fermi energy level (Figs. 3.7 G-I). In Figs. 3.7 E and F, the silicene structure retains the direct semiconductor feature. However, as the tensile strain increases, the energy band L_3 at the G-point continuously moves down and eventually crosses the Fermi energy level in figures 3.7 G-I, consequently forming indirect semiconductor.

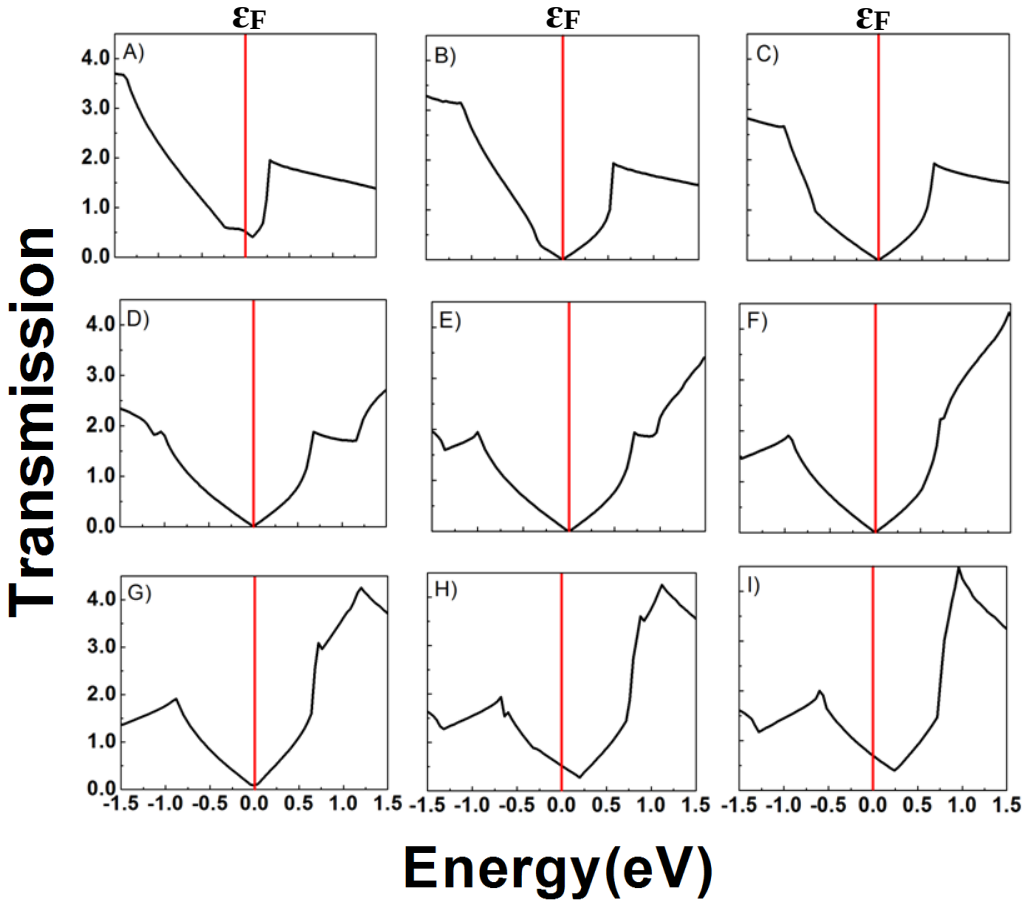

Figure 3.8 The transmission spectrum of silicene under various in-plane strain.

Figure 3.8 depicts the transmission properties at given compressive and tensile strains. The transmission spectrums are perfectly aligned with the band diagrams shown in Fig. 3.7. For figures 3.8 B-F, the minimum transmission efficiency approaches zero at the Fermi energy level, coinciding with the absence of a noticeable shift of the Fermi energy levels in figures 3.7 B-F. When a compressive strain is induced, the L_1 and L_2 bands move up in figures 3.8 A, B and C, leading to an increase of the transmission efficiency below the Fermi energy level and to the increase of the holes current. Once

the silicene energy band diagram exhibits features of an indirect semiconductor upon further increase of the compressive strain, the transmission efficiency at Fermi energy level deviates from zero. In figures 3.8 D-I, the induced tensile strain systematically increases the transmission efficiency above the Fermi energy level due to the lowering of the L_3 energy level. Further increase of the tensile strain leads to a non-zero transmission efficiency at the Fermi energy level (Figs. 3.8 G-I) which is caused by the crossing of the L_3 and the Fermi energy levels. Current-voltage (I-V) curves were calculated at given compressive (Fig. 3.9) and tensile (Fig. 3.10) strains. When the strain is beyond ±5.17%, its impact on I-V curves is significantly enhanced. This is because the silicene shows the direct semiconductor feature for strain less than ±5.17%. The transport property of the silicene structure is mainly determined by the energy band diagram in the vicinity of the Dirac cone. However, a larger strain (> ±5.17%) leads to the crossing of the L_1/L_2 or L_3 bands and of the Fermi energy level, consequently increasing the hole current and the electron current, respectively.

Systematic I-V curve calculations are first reported in this work. When larger compressive and tensile strains are induced on silicene, the current increases dramatically which shows in Fig.3.9 (black curve) and Fig.3.10 (purple curve), respectively.

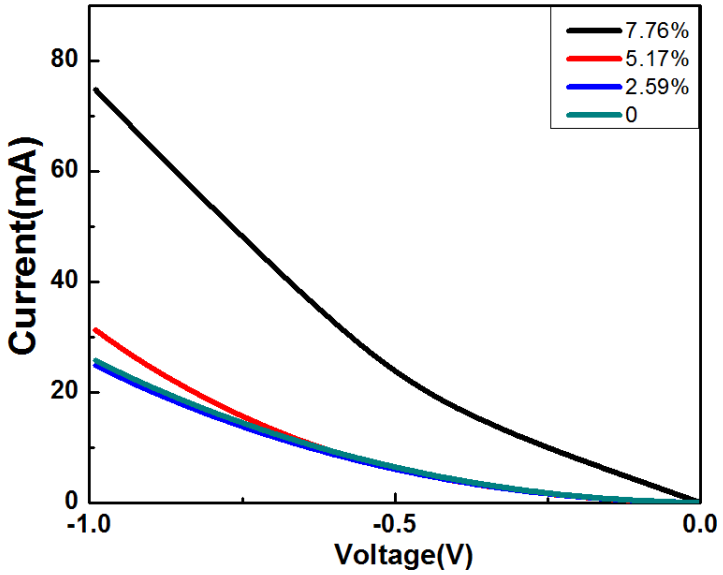

Figure 3.9 I-V curves of silicene structure under compressive in-plane strain.

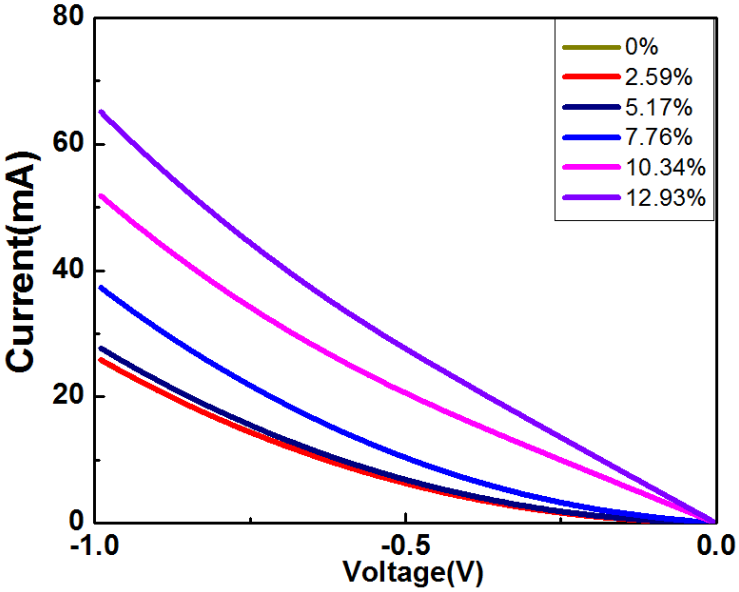

Figure 3.10 I-V curves of silicene structure under tensile in-plane strain.

3.3 Biaxial strained Bi-layered silicon film

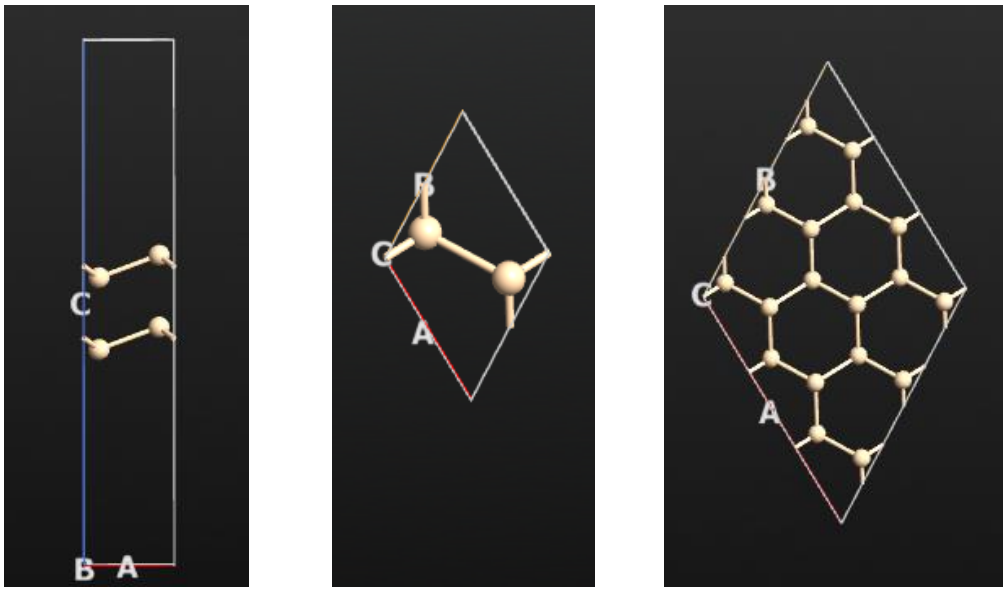

A (AA parallel)

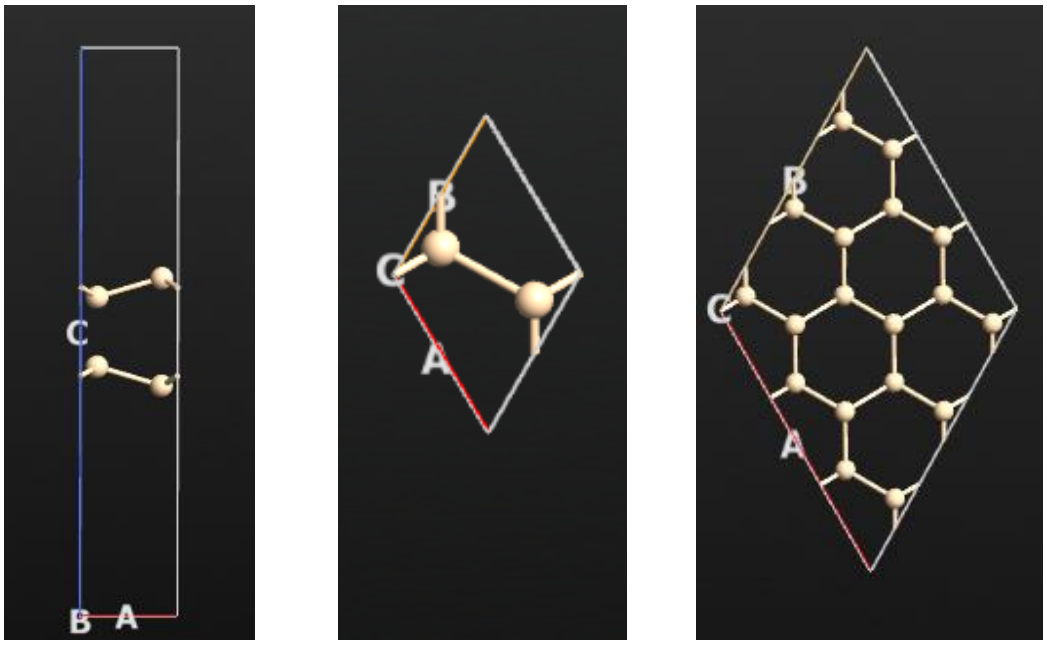

B (AA non-parallel)

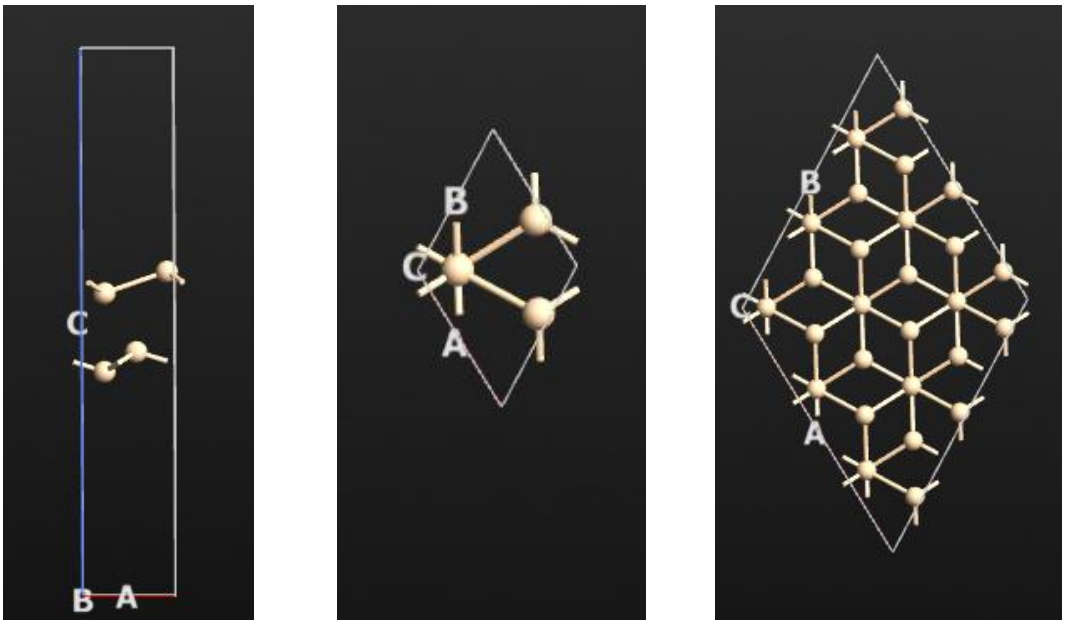

C (AB parallel)

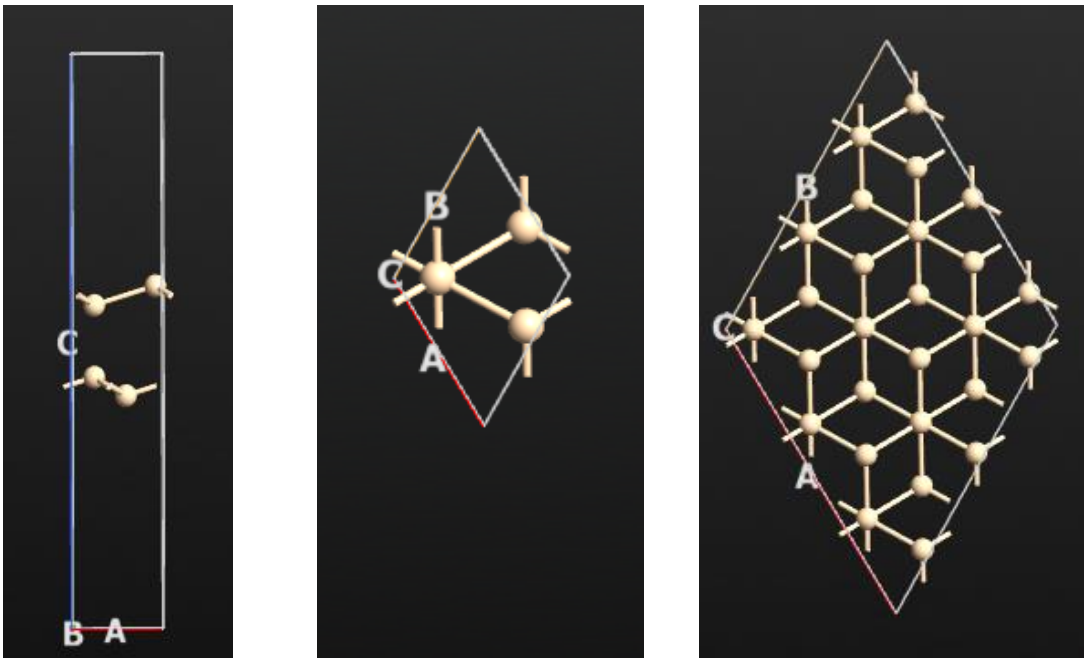

D (AB non-parallel)

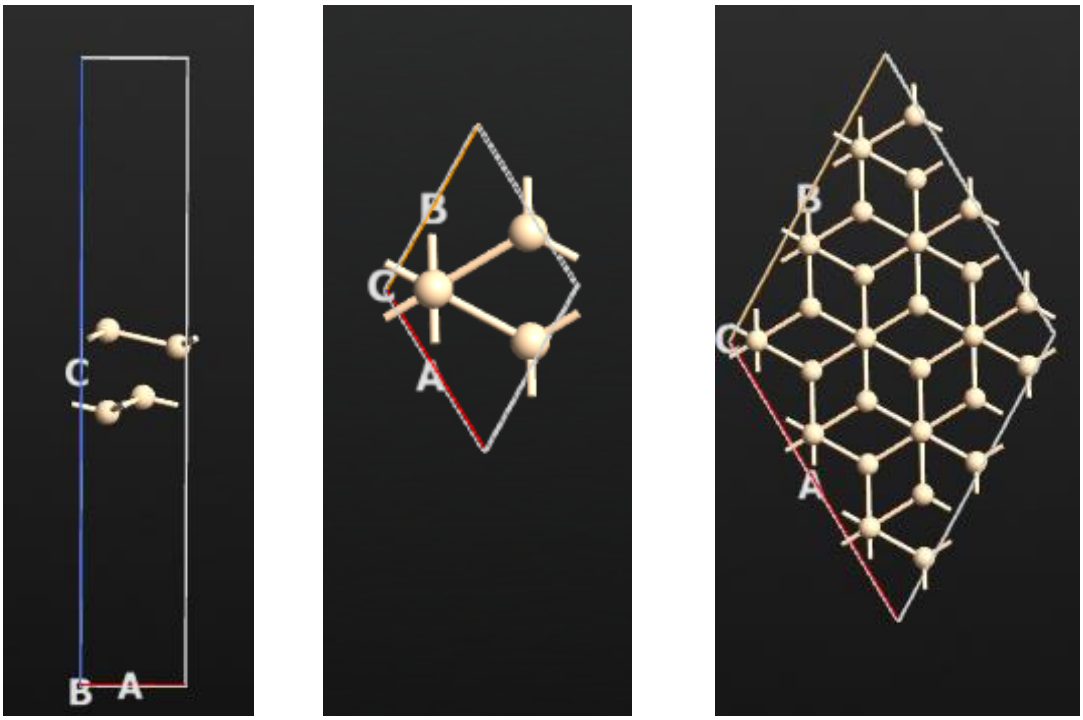

E (AB hybrid)

Figure 3.11 Bi-layered silicon film. A) Side view, top view and duplicated structures of AA-P (from left to right). B) Side view, top view and duplicated structures of AA-NP. Side view, top view and duplicated structures of AB-P. D) Side view, top view and duplicated structures of AB-NP. E) Side view, top view and duplicated structures of AB-hybrid.

3.3.1 Structural optimization of free-standing bi-layered silicon film

A bi-layer silicon film consists of four silicon atoms which can be relaxed along x-, y-, z- axis. The lattice constant of bi-layered silicon films is 3.866 Å which is the

same value as it is in silicene. DFT-GGA has been employed to obtain stabilized structures. There are five energetically stable structures obtained and, in general, they can be divided into two categories: AA and AB as shown in figure 3.11. The stability of these structures has been proved by adding a random perturbation, i.e. the silicon atoms tend to move to the original positions. The optimizations are based on reaching the minimum energy. Comparing the two categories, the total energies of AA structures are lower than of AB types. In order to form an AA structure, the initial positions of silicon atoms should be close enough to the optimized ones. The coplanar type includes coplanar parallel (AA-P, Fig. 3.11 A) and coplanar non-parallel (AA-NP, Fig. 3.11 B) structures. The non-coplanar type includes non-coplanar parallel (AB-P, Fig. 3.11 C), non-coplanar non-parallel (AB-NP, Fig. 3.11 D), and AB-hybrid (Fig. 3.11 E) structures. Table 2 shows the coordinates of all five structures, buckling height D_1 and D_2, and vertical distance D3 between the two layers.

Table 2

	Coordinates(Å)	A1(Å)	A2(Å)	A3(Å)	A4(Å)	D_1&D_2(Å)	D_3(Å)
AA-P	x	0	-0.001	1.933	1.932	0.85	1.888
	y	0	-0.009	-1.113	-1.127		
	z	0	2.738	0.850	3.589		
AA-NP	x	0	0	1.933	1.933	0.67	2.447
	y	0	-0.007	-1.115	-1.123		
	z	0	2.447	-0.670	3.118		
AB-P	x	0	-0.001	1.935	1.935	0.708	2.160
	y	0	-0.025	1.117	-1.139		
	z	0	2.867	0.708	3.650		
AB-NP	x	0	0	1.932	1.932	0.676	2.501
	y	0	-0.010	1.116	-1.126		
	z	0	2.501	-0.676	3.177		

AB-Hybrid	x	0	0	1.931	1.930	0.526	1.573
	y	0	-0.008	1.114	-1.125		
	z	0	2.611	0.526	2.099		

Figure 3.12 shows the buckling height given compressive and tensile strain. Buckling heights of AA-P and AB-NP are shown in Fig. 3.12 A. The bulking height monotonically decreases as the in-plane strain increases from compressive (negative in-plane strain) to tensile (positive strain). In addition, it turns out that the buckling height approaches zero when the tensile strain is above 7% for AB-NP and 5% for AB-P. Figure 3.12 B shows the buckling heights of AB-P, AB-NP, and AB-Hybrid. Similar to the coplanar structure, the bulking height monotonically decreases as the in-plane strain increases from compressive to tensile. However, instead of approaching zero for coplanar structure, the non-coplanar structures tend to saturate at 0.38 Å for the AB-P and the AB-Hybrid, and at 0.65 Å for AB-NP once the tensile strain is above 5%. As the band gap was only observed in coplanar structures, the following calculations are focused on the AA-P and AA-NP structures.

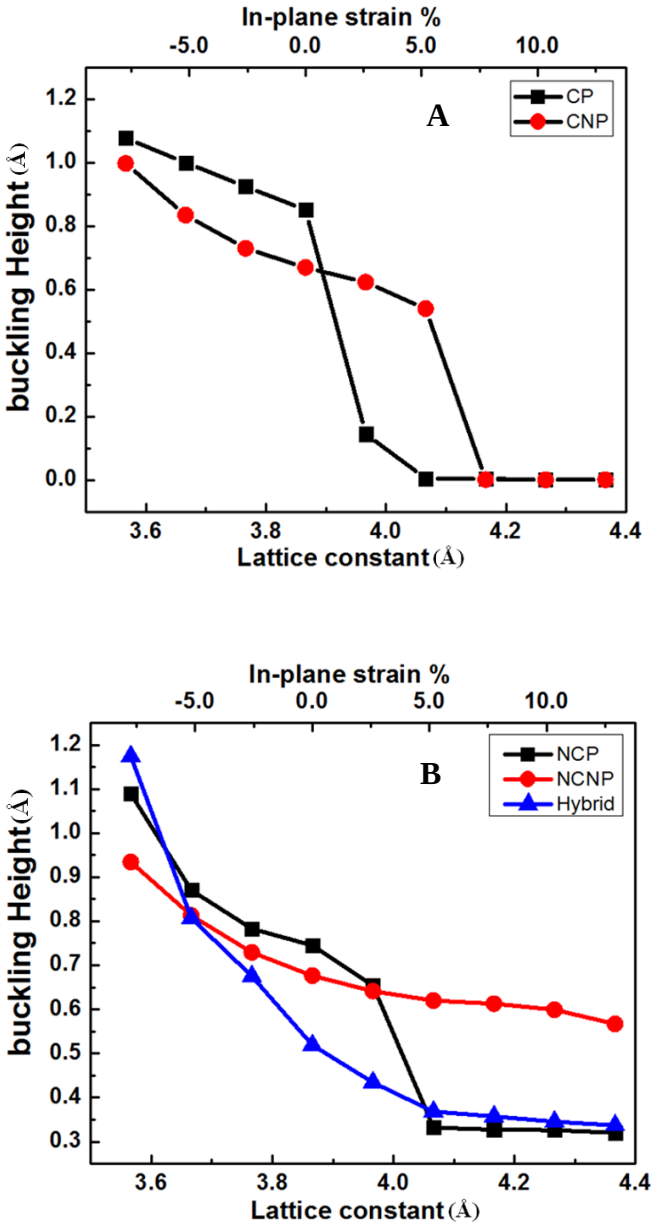

Figure 3.12 A) Buckling height of AA-P and AA-NP with induced strain. B) Buckling height of AB-P, AB-NP, AND AB-Hybrid with induced strain.

3.3.2 Energy band diagram of free-standing bi-layered silicon film

Energy band diagrams of AA-P and AB-NP are shown in figures 3.13 (AA-P) and 3.14 (AA-NP) by systematically varying the in-plane strain from compressive to tensile. In figure 3.13, a dramatic change can be seen in the AA-P's energy band diagram as tensile strain is applied to the bi-layered silicon film from the free standing and compressive strain cases. More interestingly, a sudden change of the buckling height shown in figure 3.12A occurs in the tensile strain region and the buckling height approaches zero upon further increase of the in-plane strain. Such coincidence indicates that the buckling has a significant impact on the energy band diagram in the bi-layered silicon film. A similar effect has been obtained for the AA-NP structure in figure 3.14. A rapid change in the energy band diagram is observed when the tensile strain is above 5%, at which point the buckling height also shows a big drop (Fig. 3.12A). In figure 3.11, the difference between the AA-P and AA-NP structures appears along the c-axis and the projected in-plane positions of the silicon atoms are the same. Thus, once the buckling height equals to zero, both the AA-P and AA-NP structures become identical. This is further verified by the identical energy band diagrams of the AA-P and AA-NP structures when the in-plane tensile strains are 7% (Fig. 3.13 G and Fig. 3.14 G), 10% (Fig. 3.13 H and Fig. 3.14 H), and 12.9% (Fig. 3.13 I and Fig. 3.14 I). The energy band diagrams of those flat bi-layered silicon

structures (i.e. zero buckling height) show indirect semiconductor features. The bi-layered silicon film is electrically conductive when the in-plane strain is less than 10% and becomes an indirect semiconductor as the strain reaches above 12.9%. An energy band gap up to 0.11 eV was observed in figs. 3.13 (I) and 3.14 (I).

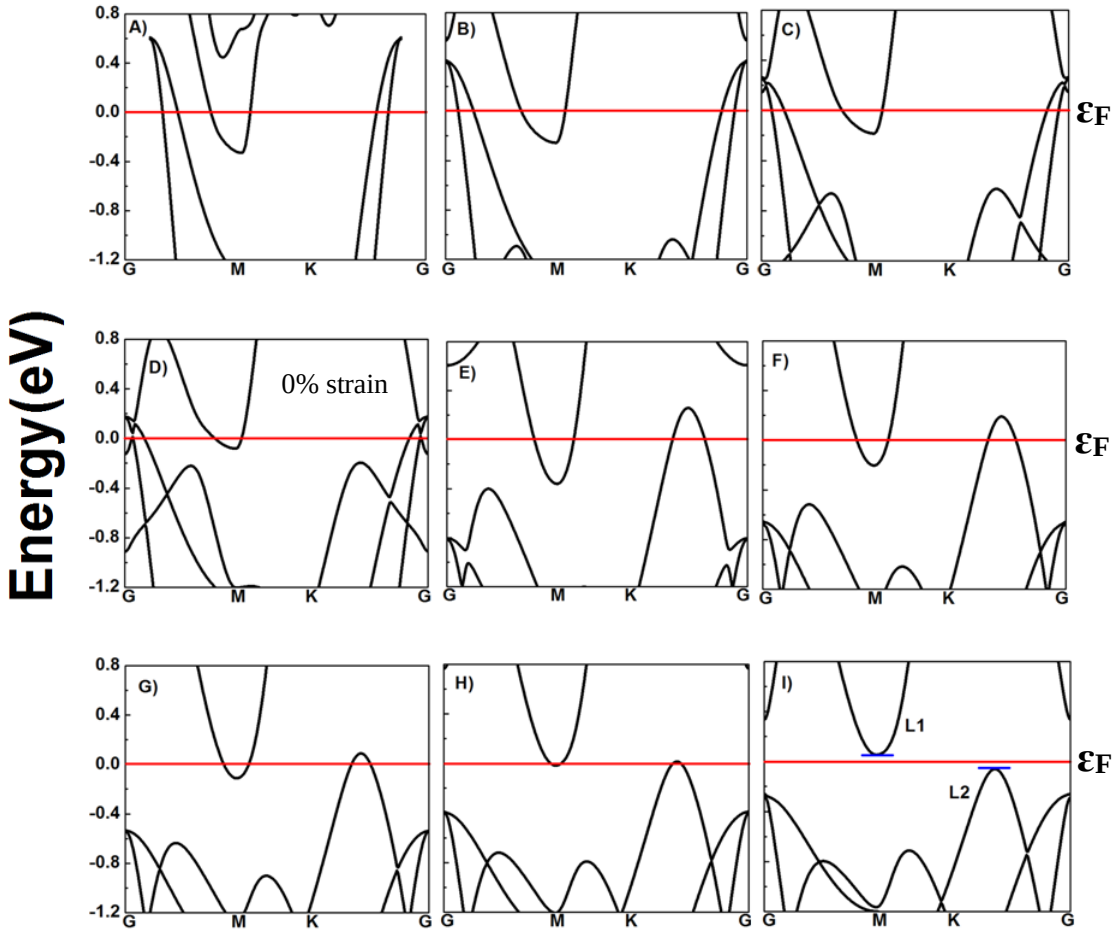

Figure 3.13 A – I shows band diagrams of AA-P by giving the lattice constant from 3.566 Å from 4.366 Å. Fermi energy level is denoted with the red line. The blue lines show the energy offset of Dirac point, energy bands L1 and L2 in (I).

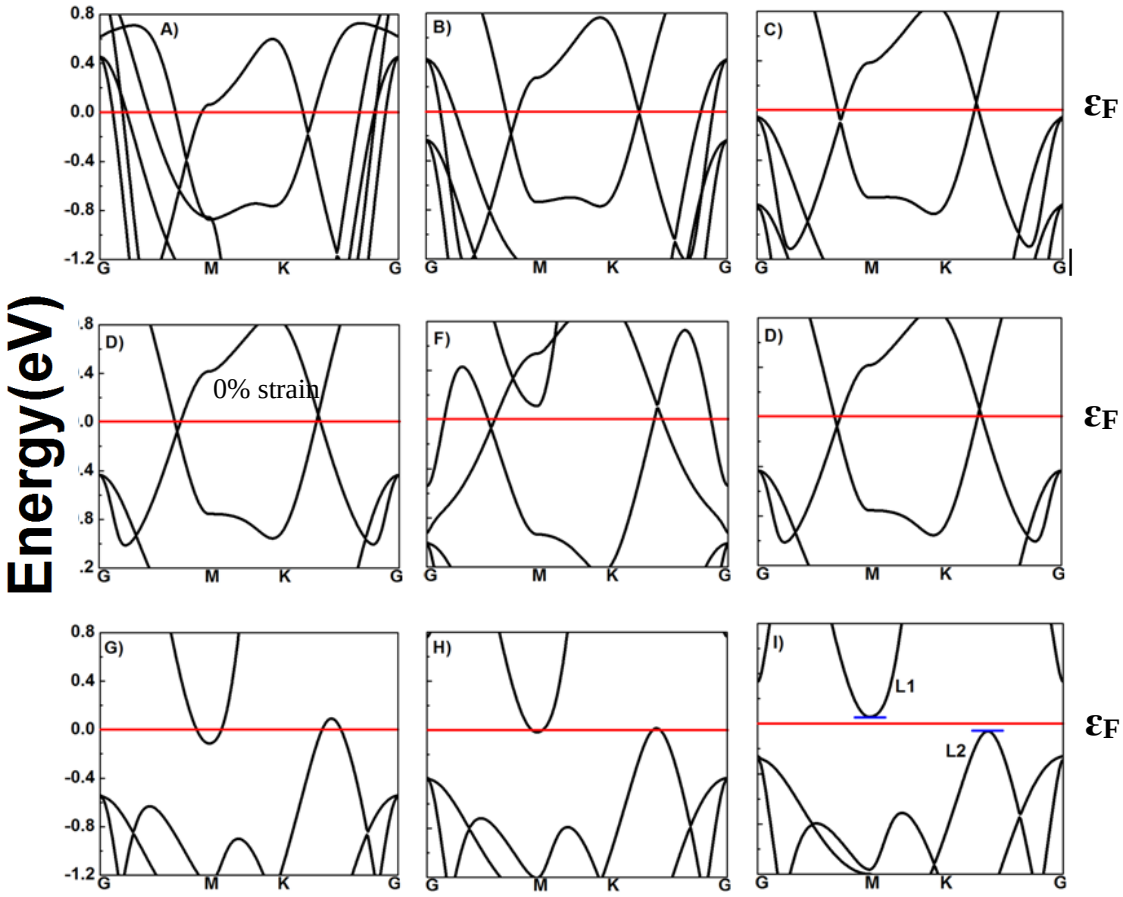

Figure 3.14 A – I shows band diagrams of AA-NP by giving the lattice constant from 3.566 Å from 4.366 Å. Fermi energy level is denoted with the red line. The blue lines show the energy offset of Dirac point, energy bands L1 and L2 in (I).

Figure 3.15 shows the band diagrams with band gap when enlarging the in-plane strain from 10.7% up to 15.4%. The opened energy band gap versus in-plane strain is

shown in Fig. 3.16. For strain in the range between 10.7% (Fig. 3.15 A) and 13.8% (Fig. 3.15 G), the energy band gap opening is almost linearly dependent on the in-plane strain. The energy band gap is given by the energy difference between the L_1 and L_2 energy bands. The energy band gap reaches a maximum of 0.168 eV when the strain equals to 14.3% (Fig. 3.15 H), and drops to zero upon further increases of the strain (Figs. 3.15 I to L). The decrease of the energy band gap in figures 3.15 H-L is caused by the lowering of the energy band L_3 below the band L_1, thus the energy band gap is counted from L_3 instead of L_1 to L_2. The energy band gap becomes zero in Fig. 3.15 L due to the crossing of the L_3 energy band and Fermi energy level.

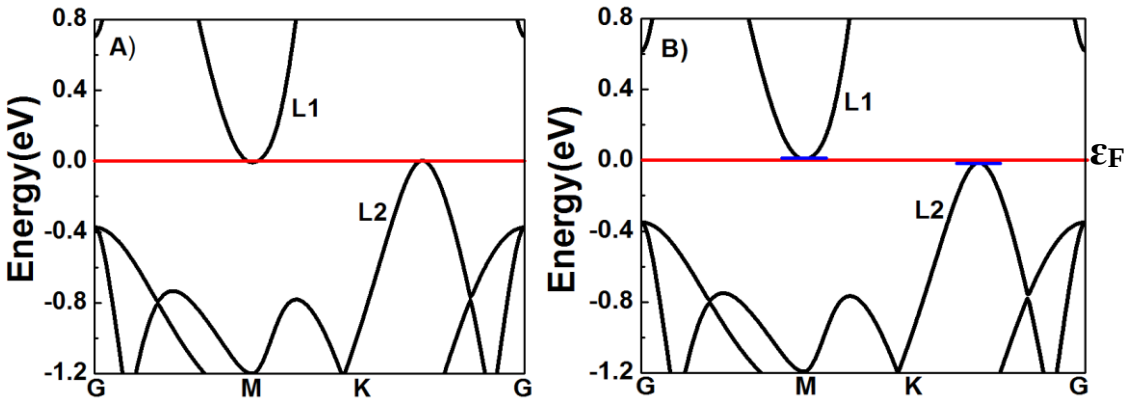

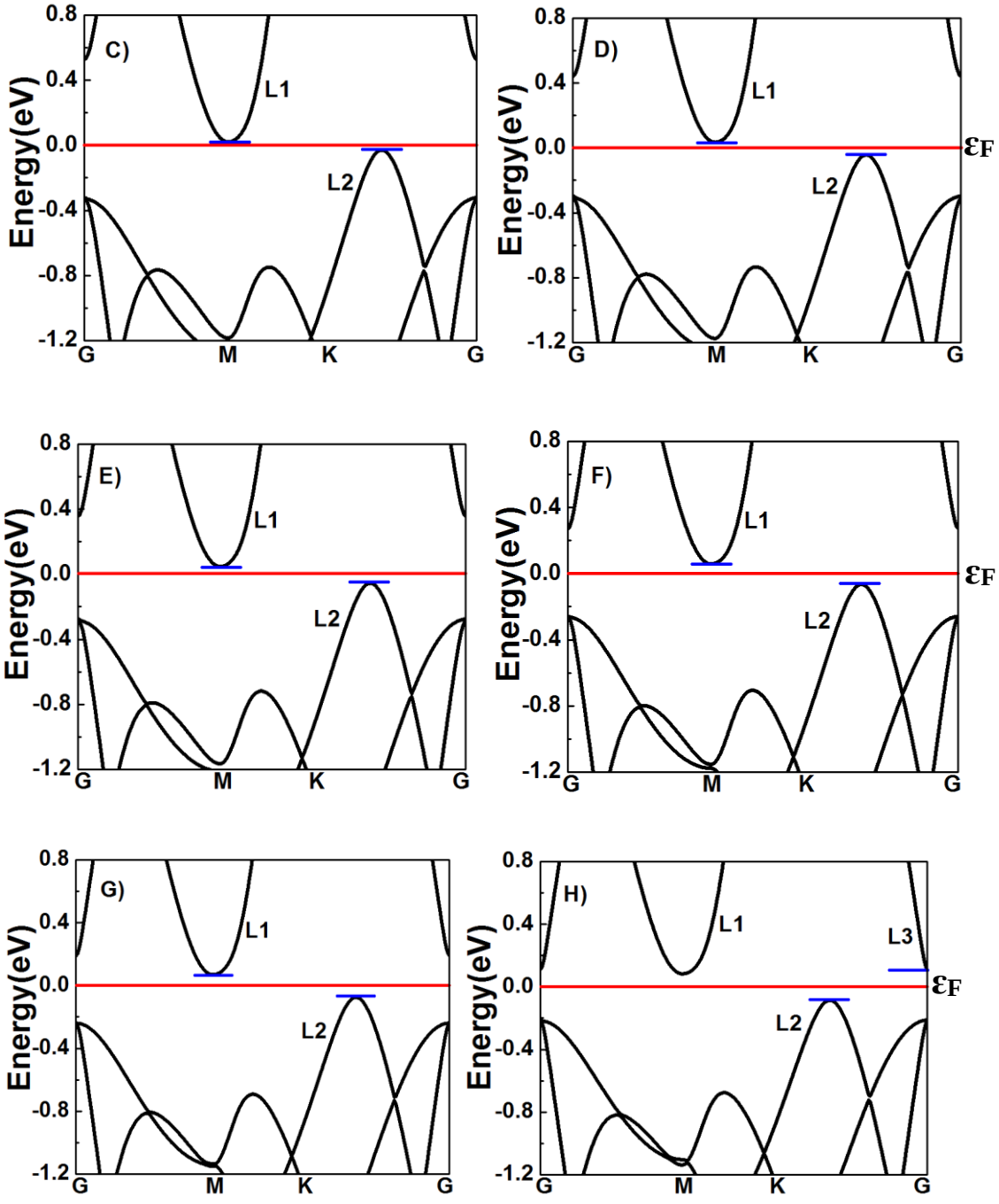
C)
D)
E)
F)
G)
H)
Energy(eV)
0.8
0.4
0.0
-0.4
-0.8
-1.2
G
M
K
G
L1
L2
L3
εF

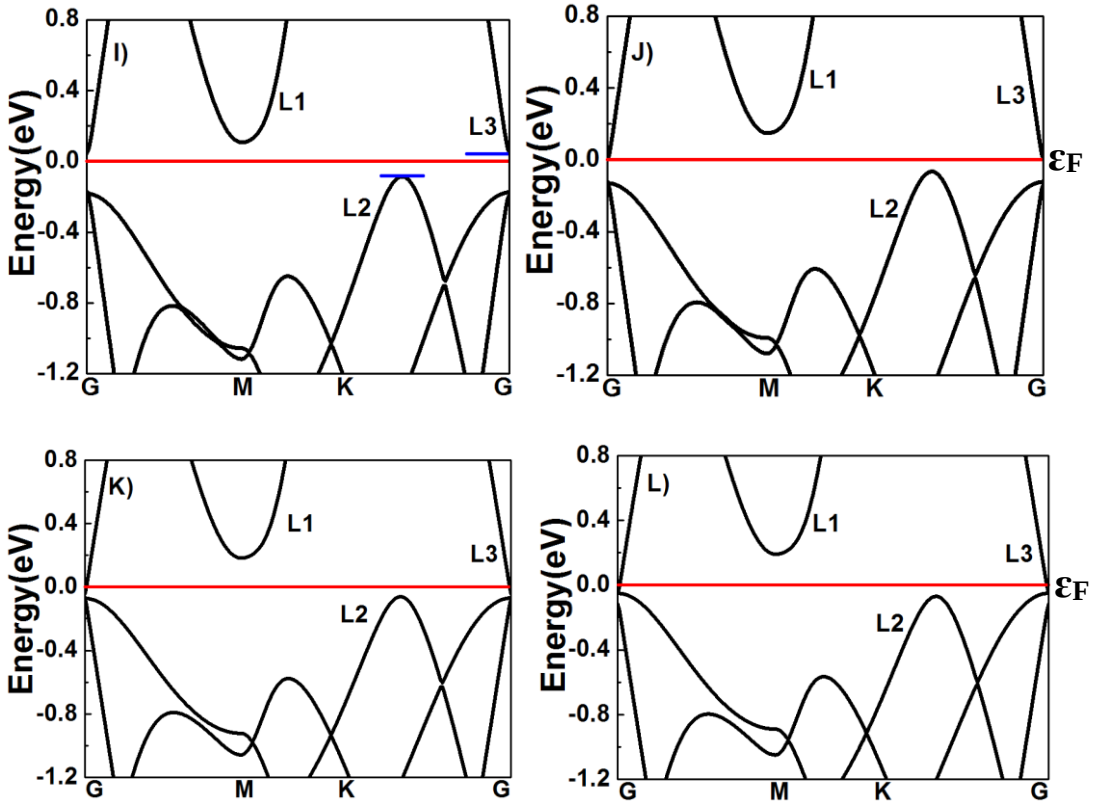

Figure 3.15 A – L shows band diagrams of AA-P and AA-NP by giving the lattice constant from 4.28 Å from 4.50 Å. Fermi energy level is denoted with the red line. The blue lines show the energy offset of Dirac point. The band gap can be observed from Fig.B to Fig.K

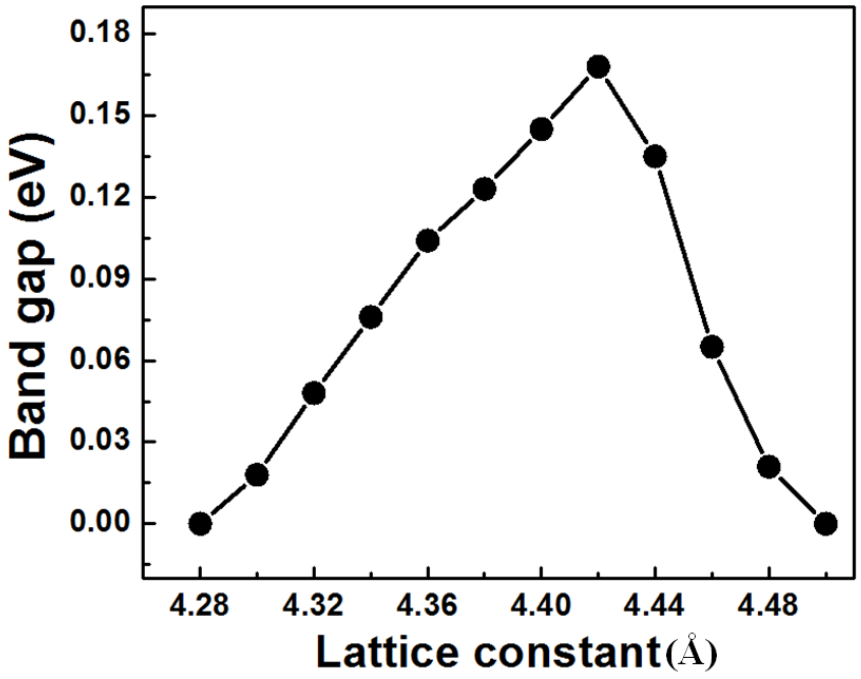

Figure 3.16 Band gap opening of AA-P and AA-NP for different tensile strain.

3.3.3 Transport properties of free-standing bi-layered silicon film

Figure 3.17 shows the transmission spectrum at the corresponding given tensile strains in figures 3.15 and 3.16. The band gap opening can be observed from figures 3.17 B–I, manifested by the zero transmission efficiency close to the Fermi energy level. This is in perfect agreement with figures 3.15 and 3.16. The current – voltage (I-V) curve and the differential I-V curve are calculated when the energy band gap reaches its maximum and are shown in Figure 3.18. Obviously due to the existence of the energy band gap, the I-V curve in figure 3.18 (A) exhibits a plateau of zero current

intensity in the vicinity of zero applied voltage. In addition, the energy band gap also leads to a peak in the differential I-V curve (Fig. 3.18 (B)).

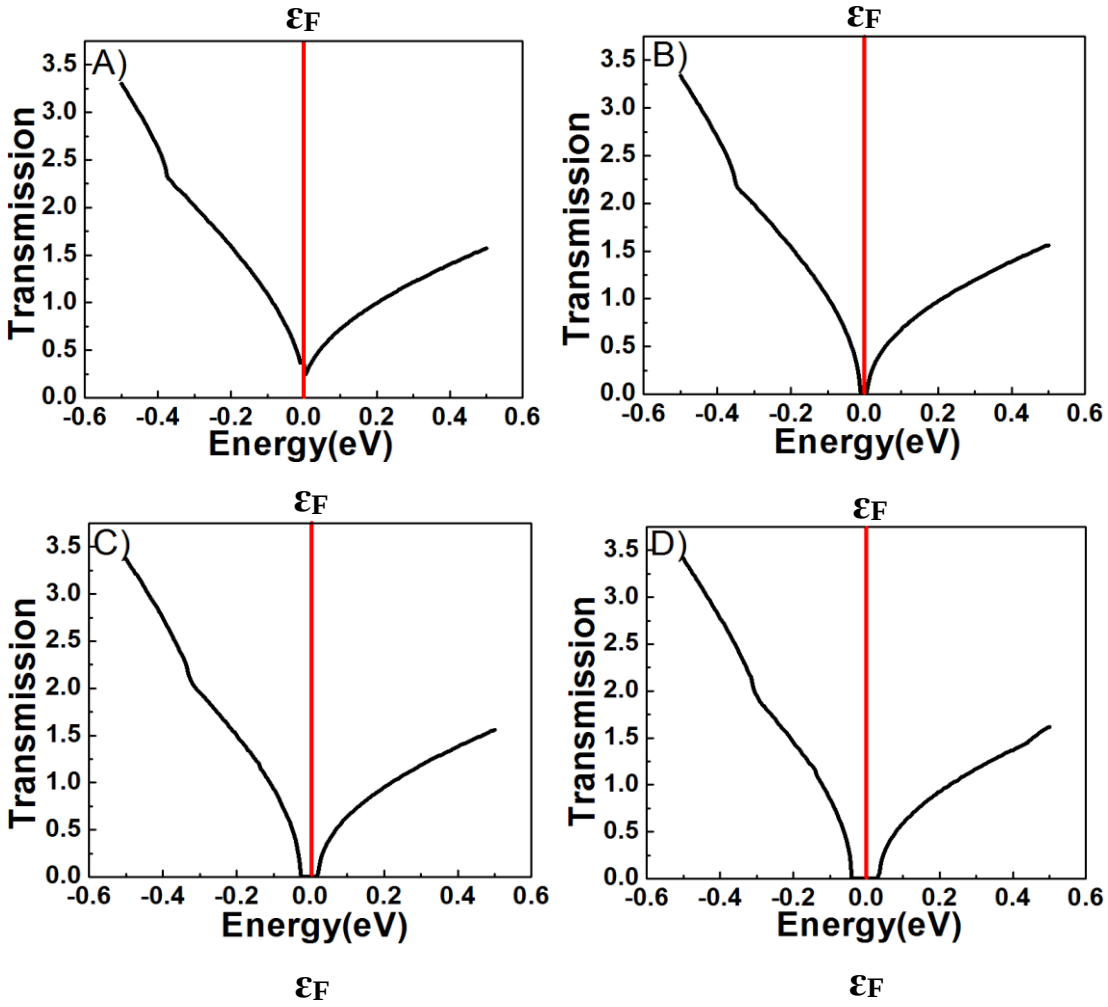

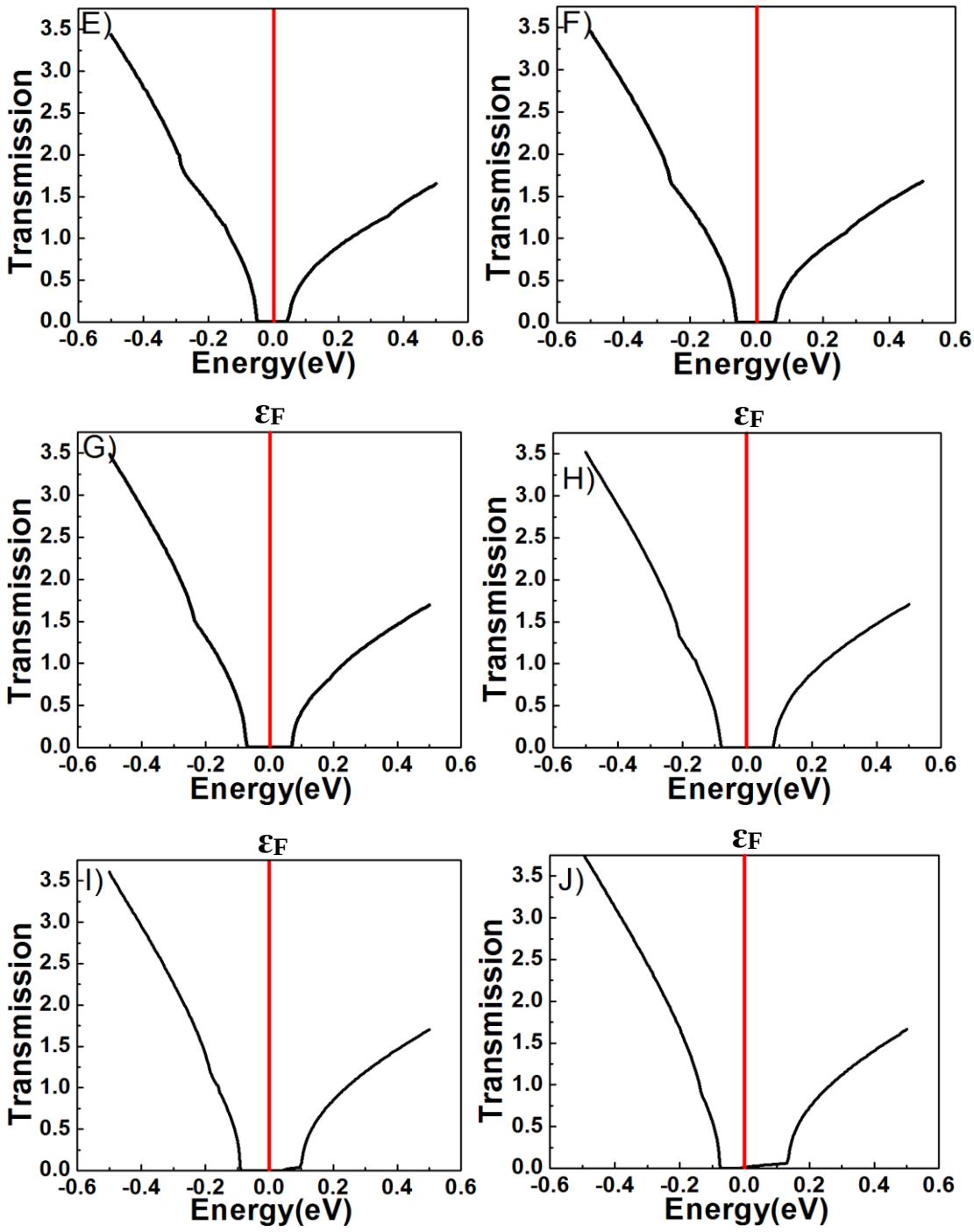
E)
F)
G)
H)
I)
J)
Transmission
Energy(eV)
εF
0.0
0.5
1.0
1.5
2.0
2.5
3.0
3.5
-0.6
-0.4
-0.2
0.0
0.2
0.4
0.6

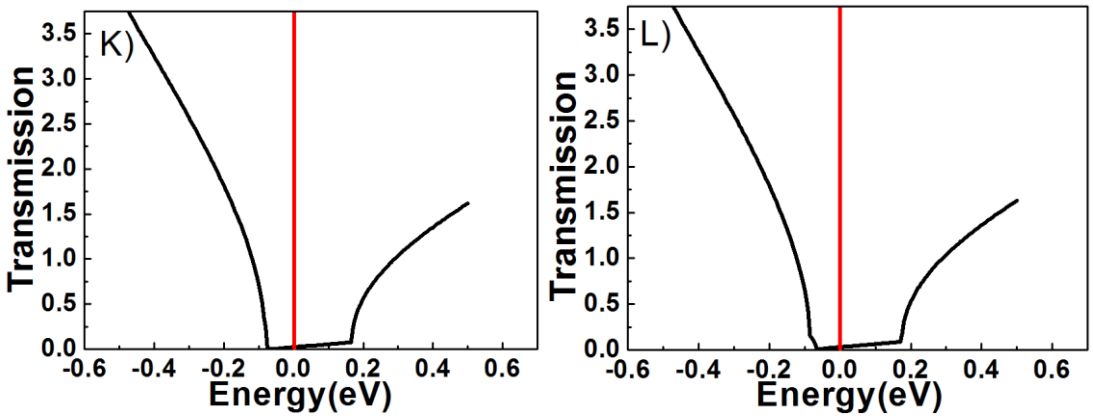

Figure 3.17 Transmission spectrum of bi-layered silicon film with tensile strain.

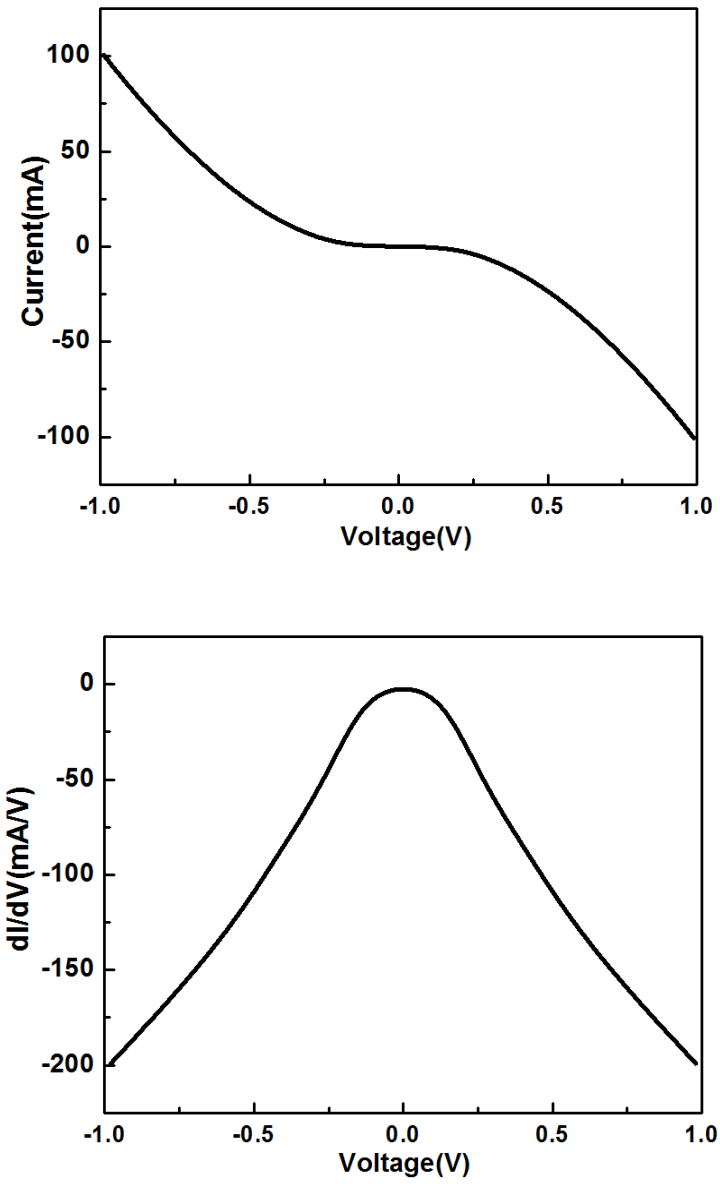

Figure 3.18 A) I-V curve of bi-layered silicon film with maximum bang gap opening.

B) Differential I-V of bi-layered silicon film with maximum bang gap opening.

Chapter 4 Selection of substrate and the analysis of experimental results

Utilizing proper substrates is a common and relatively convenient way to induce strain on graphene or graphene like materials. Silver has been investigated systematically as the substrate for silicene based on the ab initio density functional theory. Silicene can be grown on a silver substrate according to several groups, which means growing silicene on Ag substrate can exhibit many different structural phases [55]. A band gap in the range 0.1-0.4eV was obtained from the three of five systems due to the strong interaction between silicene atoms and silver atoms. However, although the value of band gap is attractive, the Ag substrate still cannot be applied on DFTs due to the metallicity of Ag. Ag is not the only substrate that people tried. More recently, ZrB_2 substrate and Ir substrate have also been reported. For instance, silicene was deposited on Ir(111) surface and annealed the sample to 670k. [15]. The paper showed that the silicon ad-layer presents a LEED pattern. Also the honeycomb feature of the system is obtained from STM. However, the gapless problem is still waiting to be solved. Recent reports proposed that the heterostructure formed by silicene and CaF_2 shows a very strong p-type self-doping feather [55]. A small band gap was obtained between π and π^*cones when the CaF_2 was induced to silicene in [111]

direction. Also, GaS was demonstrated to be a proper substrate which can form heterosheets with silicene [56]. In their work, a sizable band gap is opened at the Dirac point because of the interlayer charge redistribution. However, GaS substrate can only be obtained by mechanically exfoliation, preventing its application for silicon based mainstream semiconductor industry. Since then, researchers have been trying to investigate other semiconductor substrates, especially focusing on Group II-VI and Group III-V, e.g. AlAs (111), AlP (111), GaAs (111), GaP (111), ZnS (111), and ZnSe (111) [57]. That paper demonstrates that the properties and stability of the silicene overlayer really depends on whether the interacting top layer of the substrate shows the metallic or nonmetallic property.

4.1 Selection of substrates

Based on the calculations in chapter 3, a band gap opening has been observed in bi-layered silicon film showing hexagonal symmetry and zero buckling height. To experimentally synthesize such a structure, the substrates on which the bi-layered silicon film is grown on must be properly selected regarding the structural symmetry and lattice constant. The former assures the desired symmetry of the bi-layered silicon film, the latter induces strain/stress to the bi-layered silicon film to flatten the buckled structure.

As the bi-layered silicon film possesses hexagonal symmetry, naturally the substrate should have the similar structural symmetry. Many semiconductor materials are based in a close-packing of a single kind of atom, or a close-packing of large ions with smaller ions filling the spaces between them. The two most common structures are zinc-blend (ZB, Figure.4.1 A) and hexagonal close-packed (HCP, Figure.4.1 B). In this work, all the simulations are focused on HCP substrates. Depending on the stacking order, HCP could have various structures such as 2H (Fig. 4.2 (a)), 4H (Fig. 4.2 (b)) and 6H (Fig. 4.2 (b)). To simplify the computation, the 2H structure is chosen in the simulations, which is also called Wurtzite structure. The stacking sequence of Wurtzite structure is ABABABA. In our simulations, four atomic layers have been constructed with the bottom atomic layer fixed.

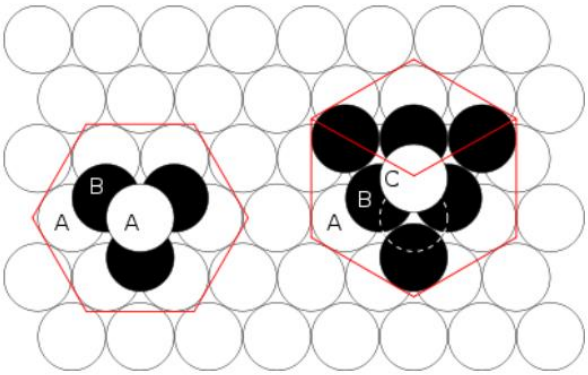

Figure 4.1 A) close-pack structure of hexagonal. B) close-pack structure of Zinc blende.

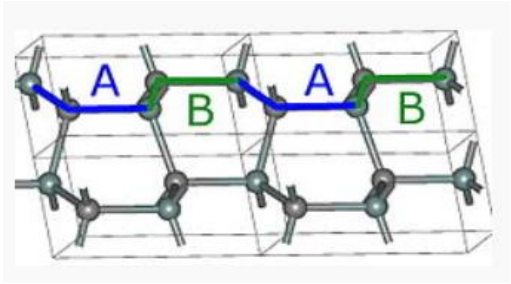

A

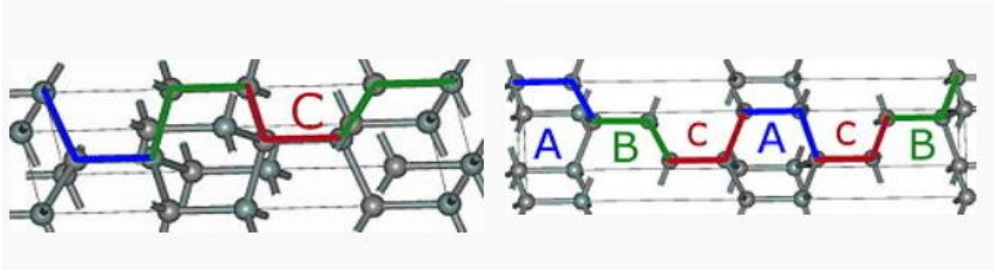

B C

Figure 4.2 A) Atomic structure of 2H. B) Atomic structure of 4H. C) Atomic structure of 6H.

The other critical feature needed to obtain a band gap opening in the calculations in chapter 3 is to induce an in-plane strain to eliminate the buckling height of the bi-layered silicon film. In order to induce an in-plane strain, the lattice constant was changed as we did for silicene. For free standing bi-layered silicon films, the buckling height monotonically decreases as the in-plane strain becomes larger and eventually approaches zero. The energy band gap starts to open as the applied in-plane strain reaches above 10.7% and below 15.4% (Fig.3.15). A large variety of substrates (listed

in table 3) having the Wurtzite structure have been examined. Due to the different lattice constants, the in-plane strain can be varied from -33.9% ~ 18.6% as shown in Figure 4.3, which covers the entire range of the in-plane strain required to generate the energy band gap for free standing bi-layered silicon film.

It is well known that the cubic phase is the most popular form for semiconductor materials. Systematic studies have been experimentally performed and reported in [58], showing that conversion of bulk structures from ZB to WZ is feasible. For example, in order to produce GaAs Wurtzite structure, the ZB structure is first transferred to an orthorhombic structure under 24 GPa hydrostatic pressures, and then transformed to a SC16 structure by heat treatment under pressure ~14 GPa. Finally, the WZ phase can be formed by further heat treatments [59].

WZ models of a variety of listed semiconductor materials in Table 3 have been established in ATK. As an example, figure 4.4 shows the atomic WZ structure of an InAs substrate with the lattice constant of 4.284 Å and the bond length of 2.614 Å. The WZ structure consists of four atomic layers and is optimized by allowing free relaxation of all four atoms along x-, y-, and z- axis. The atomic structures have been optimized using both the local density approximation (LDA) and the generalized gradient approximation (GGA), and the results obtained from both approximations have a little difference due to different approximations. All the following calculations

are performed based on GGA result due to the more accurate approximation. In the calculations, periodic boundary condition was chosen to allow self-consistent solving of the Poisson equation using the fast Fourier transform solver. The other parameters in the calculations are chosen to be the same as in Chapter 3. The energy band diagram of the InAs WZ structure is shown in Fig. 4.5. The InAs WZ is a direct band gap material with an energy band gap of 0.69 eV.

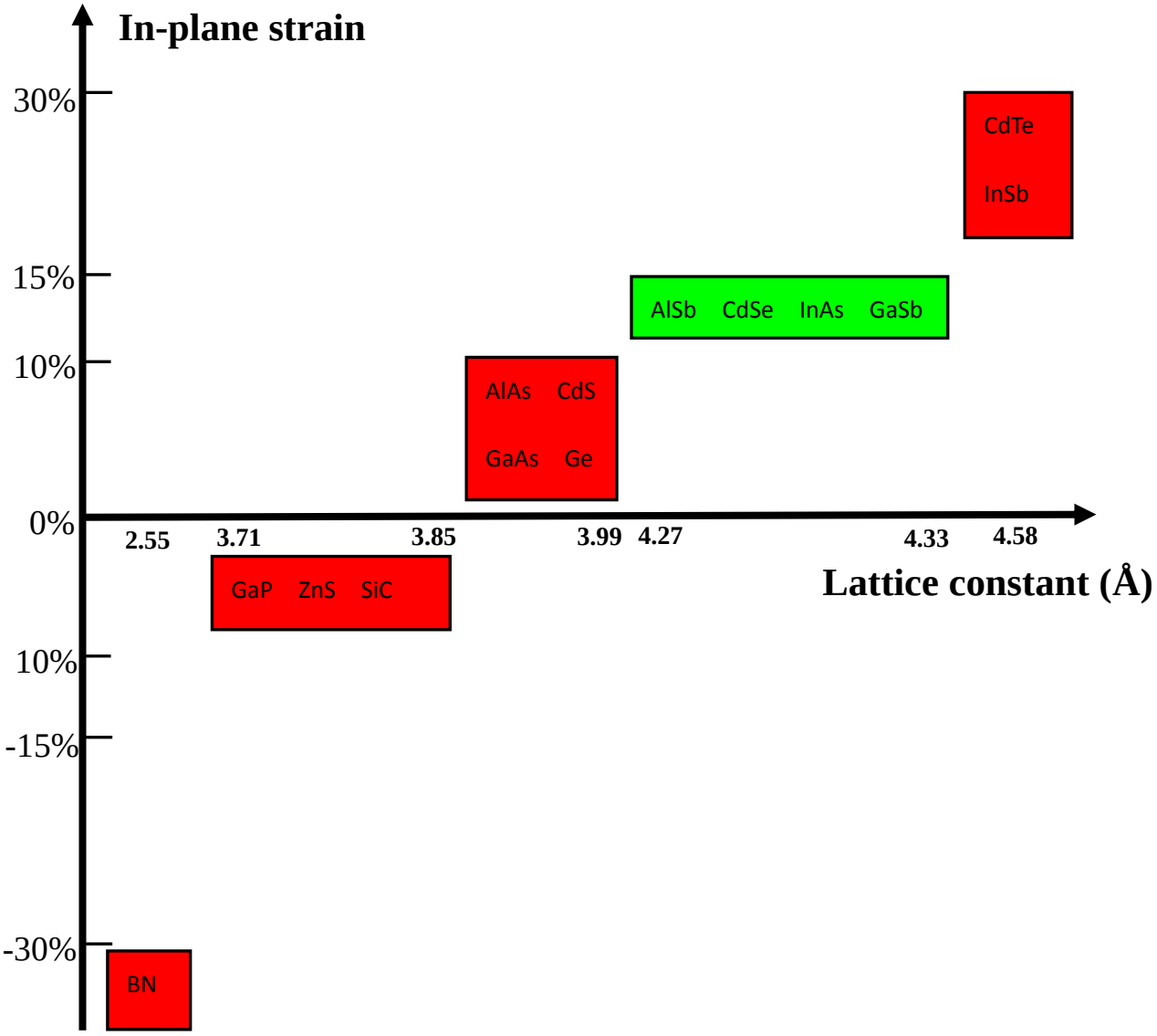

Figure 4.3 Strain provided to bi-layered silicon film from WZ substrates.

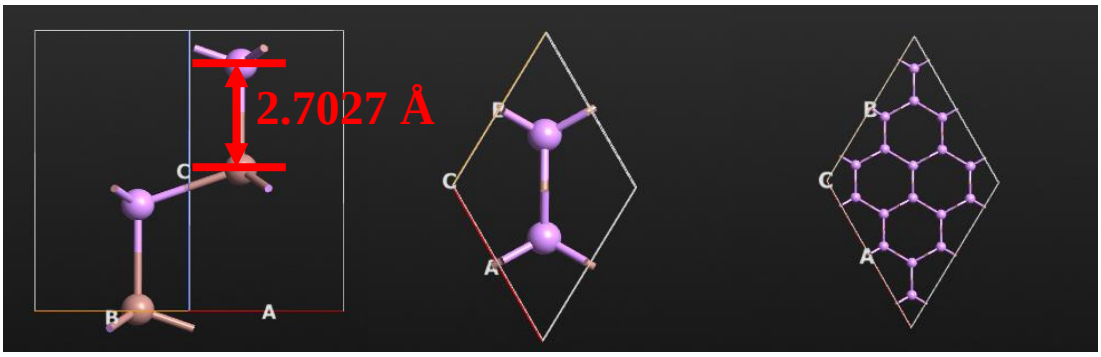

Figure 4.4 WZ atomic structure side view, top view, and duplicated 3by3 (from left to right).

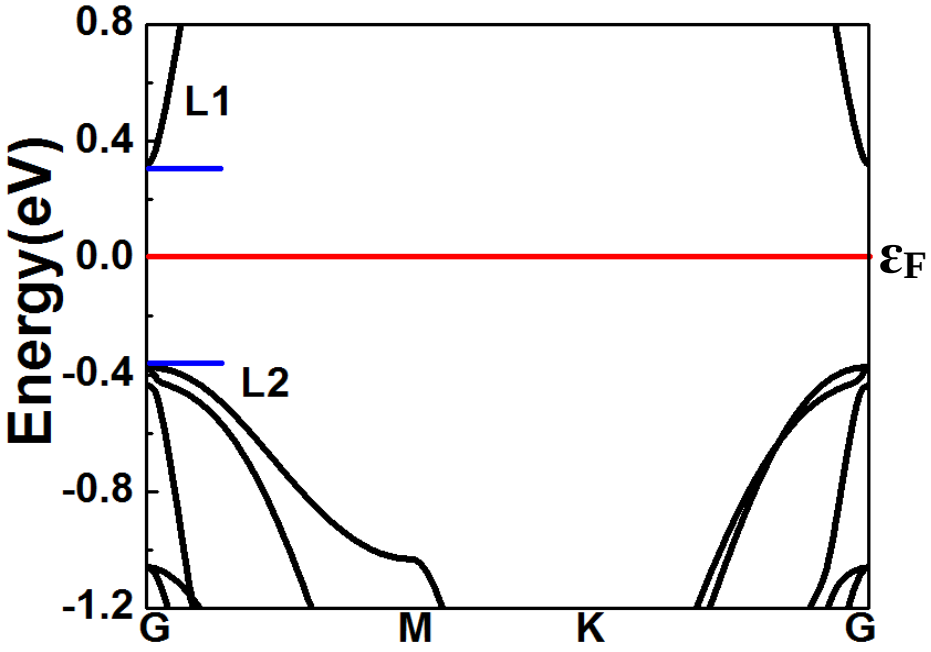

Figure 4.5 Band diagram of WZ InAs.

Table 3

	Lattice constant（Å）	Bond length（Å）	In-plane strain （%）
AlAs	3.974	2.434	2.79
AlSb	4.339	2.656	12.23
BN	2.557	1.565	-33.86
BP	3.209	1.965	16.99
CdS	4.115	2.519	6.44
CdSe	4.279	2.620	10.68
CdTe	4.583	2.806	18.55
GaAs	3.998	2.448	3.41
GaN	3.18	1.989	17.74
GaP	3.855	2.360	0.28
GaSb	4.327	2.649	11.92
Ge	4.001	2.450	3.49

InAs	4.284	2.614	10.42
InP	4.150	2.541	7.35
InSb	4.581	2.805	18.49
SiC	3.705	1.883	4.16
ZnO	3.274	2.005	15.31
ZnS	3.826	2.342	1.03

4.2 Structural optimization of bi-layered silicon film

A variety of WZ structures with various lattice constants were used as substrates to induce either tensile or compress strains to the silicon layer. In general, at least four atomic layers are required to adapt the strain relaxation in the substrate. During the structural optimization, the bottom atomic layer is fixed to stand for multiple solid layers substrate while the other three atomic layers are allowed to relax along x-, y-, and z-axis. The top- and side- views of a WZ substrate is shown in figure 4.6.

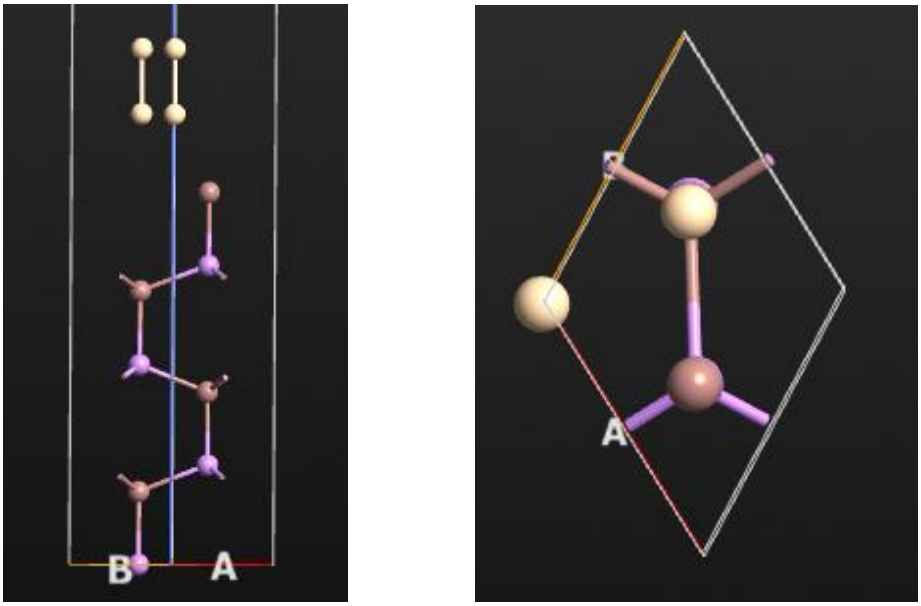

Figure 4.6 The combination of InAs substrate and bi-layered silicon film (side view-left, top view-right).

From the calculations in chapter 3, each layer consists of two silicon atoms. To form a bi-layer structure, four silicon atoms have been used with the initial positions shown in figure 4.7. The vertical height between the first silicon layer and the substrate is 2.8 Å, and the distance between the two silicon layers is 2.37 Å. Within each silicon layer, the two silicon atoms are set to flat, i.e. the same height along the c-axis. The lattice constant along the c-axis is set to 40 Å to avoid inter-layer interaction. In the calculations, periodic boundary condition was chosen to allow self-consistent solving of the Poisson equation using the fast Fourier transform solver. The atomic structures

have been optimized using the generalized gradient approximation (GGA). After structure's optimization, a perturbation was applied to further verify the stability of the structure.

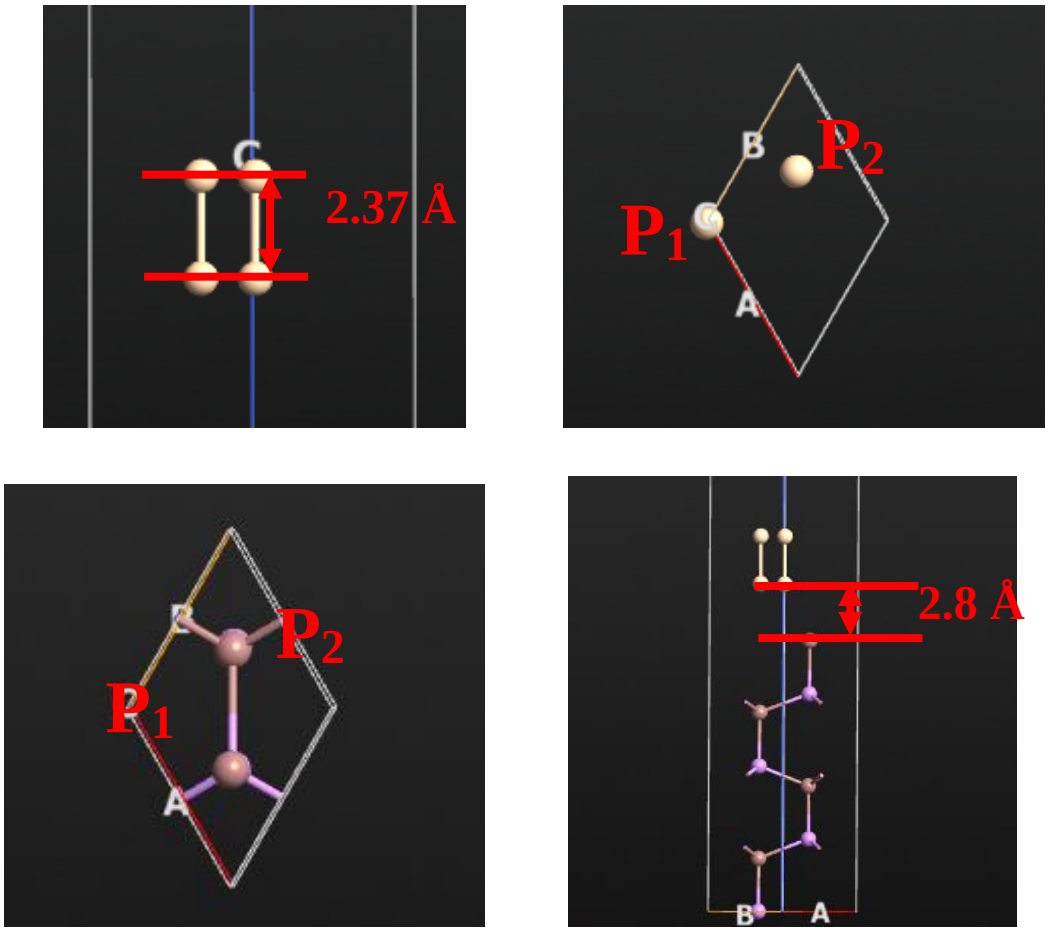

Figure 4.7 Initial position of four silicon atoms.

Structural optimization of the bi-layered silicon has gone through the entire list of the materials shown in figure 4.3. The silicon layer on all these substrates exhibits hexagonal symmetry. Depending on the induced strain/stress by the substrates, the

height of the buckling varies for different substrates, as shown in figure 4.8. The general trend is similar as the free standing bi-layered silicon film discussed in chapter 3: above a critical value of tensile strain ~7%, the buckling height is saturate.

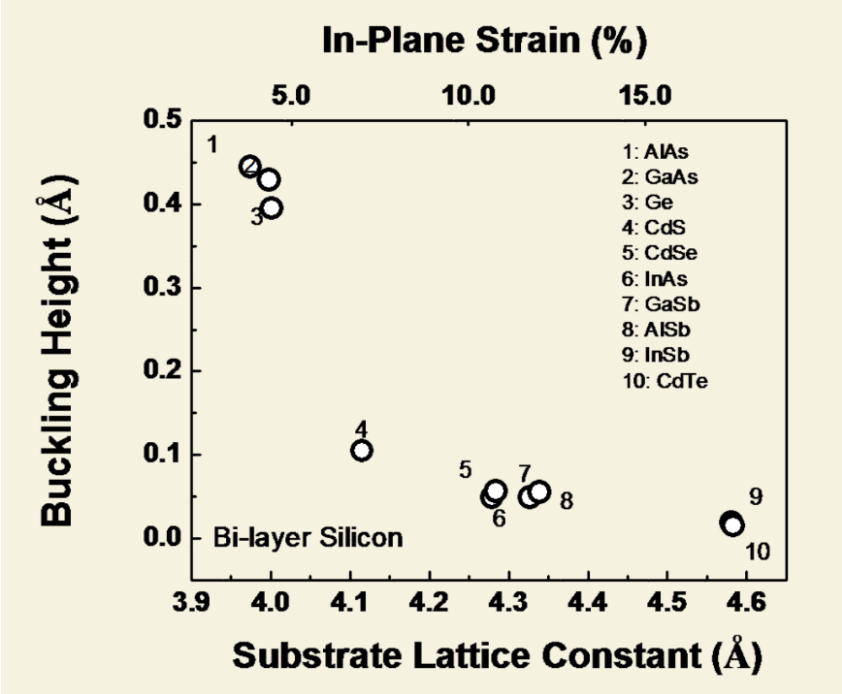

Figure 4.8 Buckling height of bi-layered silicon film for different substrates.

As discussed in chapter 3, inducing 10~15% tensile strain to two dimensional bi-layered silicon will lead to energy band gap opening. Shown in figure 4.3, four materials InAs, GaSb, AlSb, and CdSe are able to produce tensile in-plane strain to the atop silicon layer. Figure 4.9 shows the optimized structure of the bi-layered silicon film on InAs substrate as an example and Figure 4.10 shows the optimized substrate of InAs, which is a little bit higher than original one along z axis.

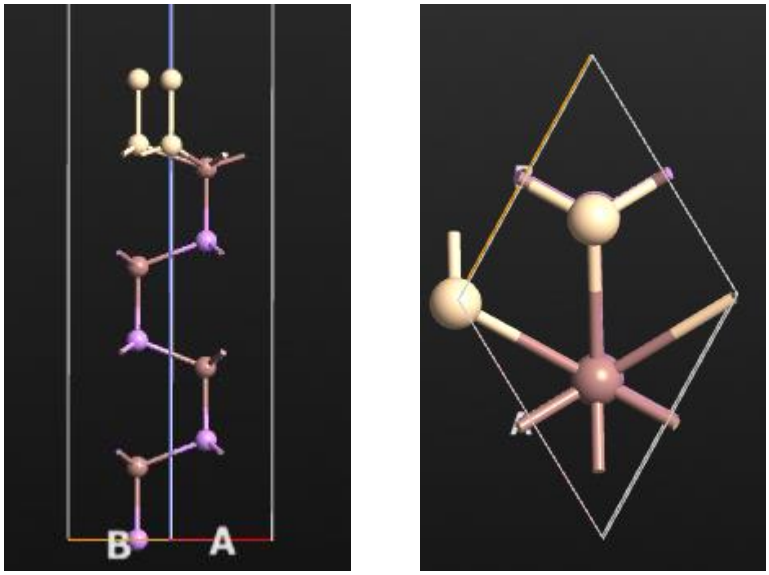

Figure 4.9 Optimized bi-layered silicon film with InAs substrate (side view and top view).

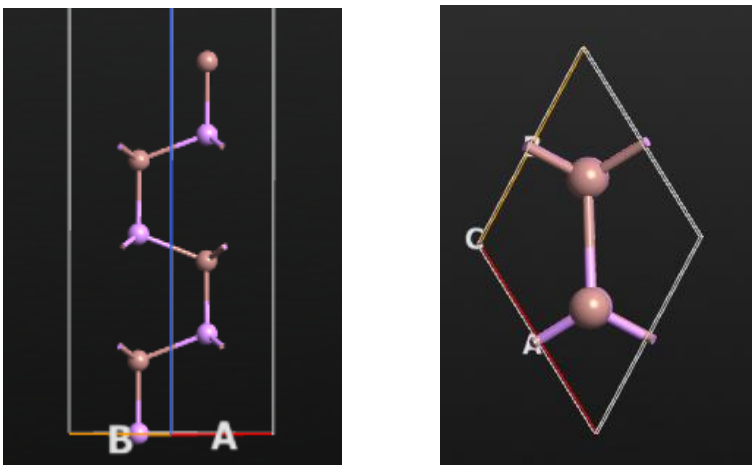

Figure 4.10 InAs substrate after optimization (side view and top view).

4.3 Strain-induced energy band gap opening and the transport property of the bi-layered silicon film

To open the energy band gap in the bi-layered silicon film, tensile strain in the range between 10% and 15% needs to be induced. Considering the free standing lattice constant of silicon is 3.866 Å, the lattice constant of the substrate must be in 4.252 Å ~4.446 Å in order to satisfy the requirements of strain. By searching the most popular semiconductor materials, four materials InAs, GaSb, AlSb, and CdSe have been found with proper lattice constants.

In the model, the substrate is considered as an eight layer stack with the bottom layer fixed. Such structure does not have the periodicity along the c-axis due to the external

20 Å vacuum to avoid the interlayer coupling effect. Thus, after structural optimization, the substrate has been removed to obtain solely the energy band diagram of the bi-layered silicon. The energy band diagrams of the optimized bi-layered silicon structure on InAs, GaSb, AlSb, and CdSe are shown in figures 4.11. As strain above 10.68% (the lowest in the four materials), the noticeable band gap can be observed.

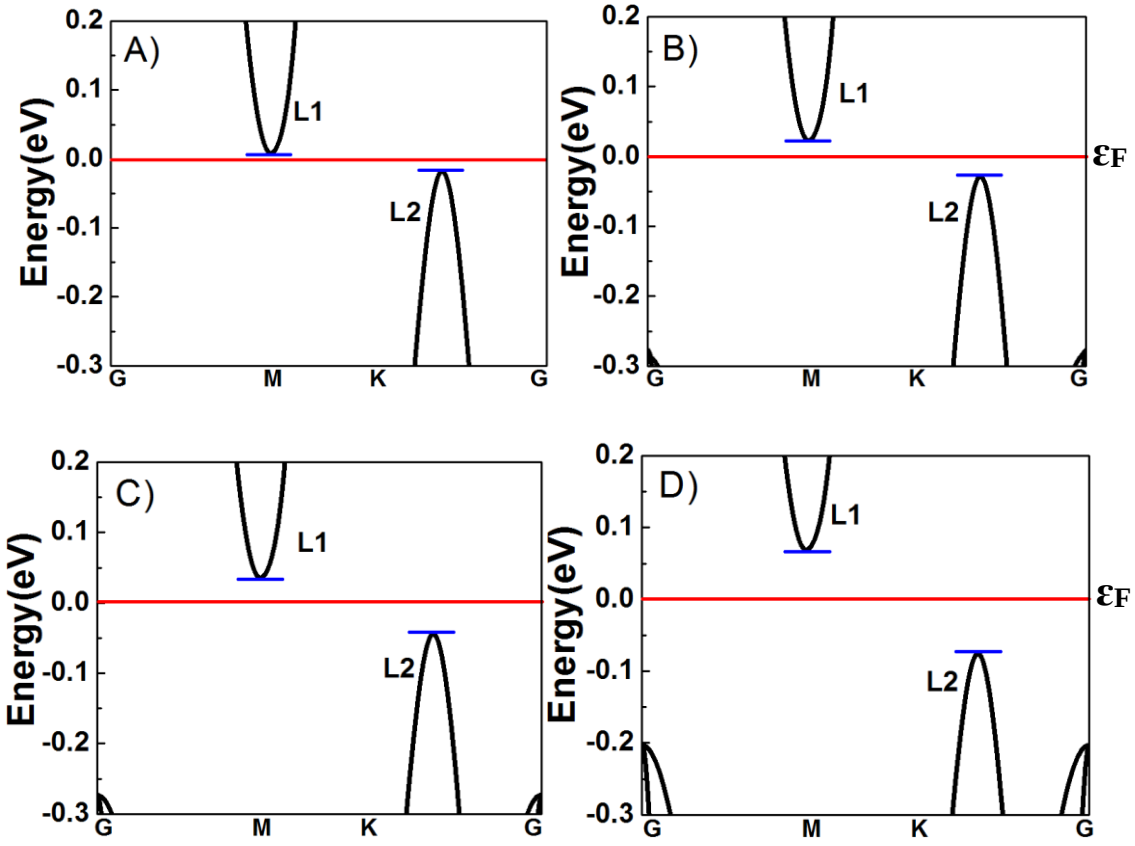

Figure 4.11 Band diagrams of CdSe, InAs, GaSb and AlSb.

To further increase the strain on InAs, GaSb, and AlSb, the energy band gaps are opened wider. In addition, the energy band diagram shows the indirect semiconductor feature. Once the strain reaches 18.49% (InSb), the L_3 band moves up and eventually crosses the Fermi energy level. As a result, the energy band gap disappears. On the other hand, below 3.41% (GaAs), the strain is insufficient to open the energy band gap. Figure 4.12 shows the band gap opening versus substrates with various lattice constants. The results are in a very good agreement with those obtained from free standing bi-layered silicon structure in chapter 3. Transmission efficiency and the I-V curves of the optimized bi-layered silicon structures are shown in figures 4.13 and 4.14, which coincide with the energy band diagrams.

The band diagrams were calculated based on bi-layer silicon films after removing those substrates since it is very difficult to analysis the entire system. In the figure 4.12, the band gap of bi-layered silicon film obtained based on the four substrates are a little higher than those in the free-standing structures. The reason for that because in the structural optimization, the interaction potential is calculated while including the effect of substrates. When calculating the band diagrams, we use the same original potential, which therefore still contains the influence of substrate on electronic properties and is different from the free standing potential.

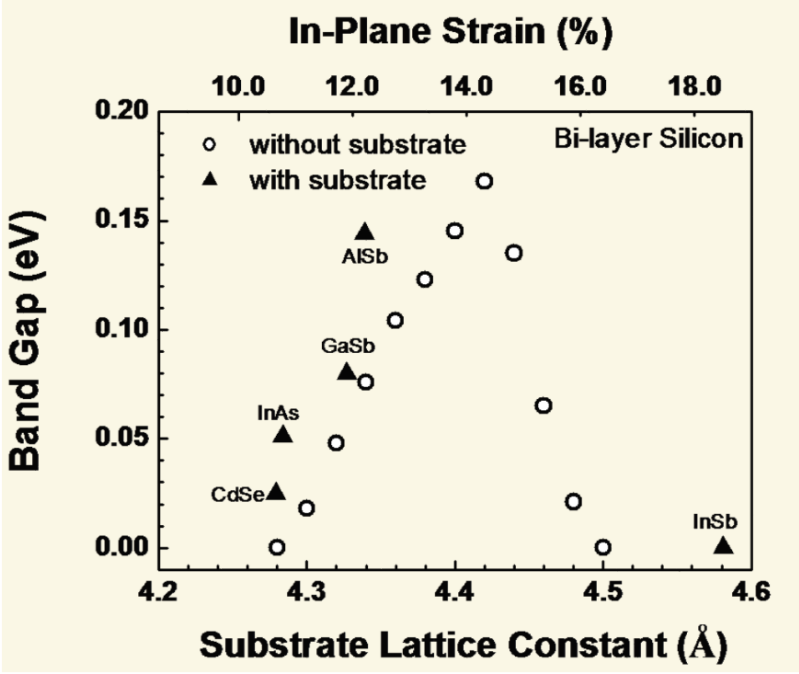

Figure 4.12 Band gap opening with different substrates.

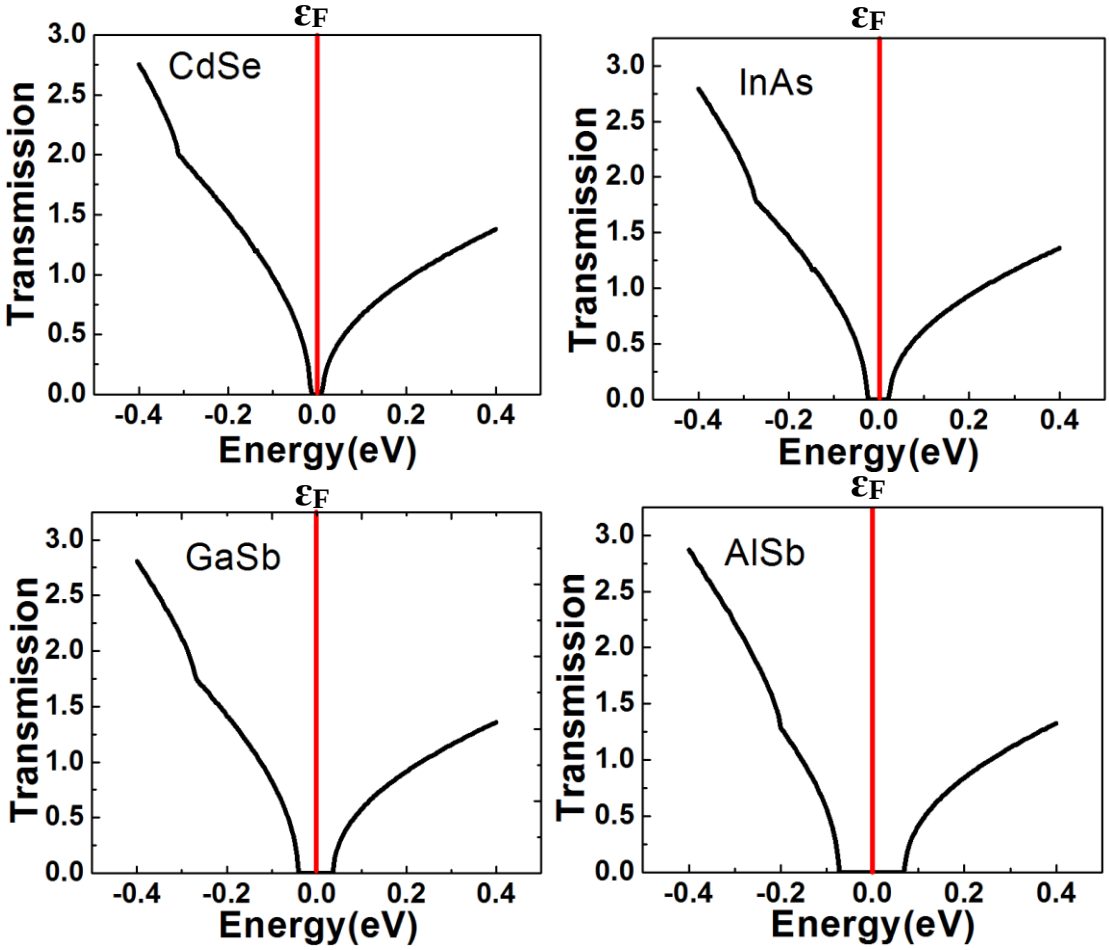

Figure 4.13 Transmission spectrum of CdSe(A), InAs(B), GaSb(C), and AlSb(D).

Fig.D shows the largest band gap due to the largest lattice constant.

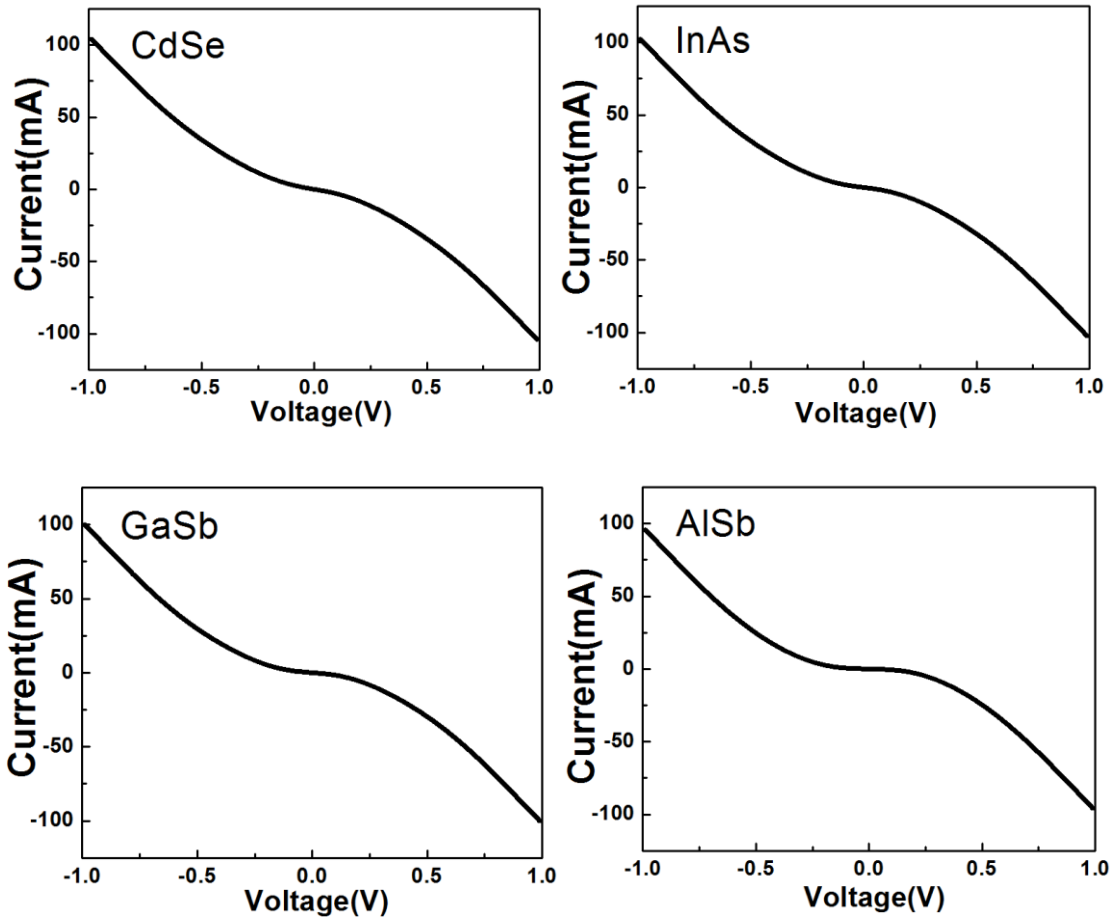

Figure 4.14 I-V curve of CdSe(A), InAs(B), GaSb(C), and AlSb(D).

Chapter 5 Summary and future work

Summary

In this work, the atomic structures of both silicene and bi-layered silicon film were investigated. The transmission properties were also performed on both structures by adding compressive and tensile strain. The CNP and CP structures showed the semiconductor properties when the tensile strain is above 10%. After that, numerous substrates of semiconductors, which have WZ structure, were tested to provide the tensile strain. Finally, CdSe, InAs, GaSb, and AlSb were able to provide enough strain and generate a band gap opening based on bi-layered silicon film. The maximum band gap can be obtained from AlSb substrate is 0.144 eV.

Future work

As the band gap was observed from bi-layered silicon film by using WZ substrates, further work will be still focusing on the selection of substrates. Although some semiconductor materials can provide enough tensile strain, the manufacturing process of WZ structure is still very complicated. As the feature of bi-layer silicon was developed, any substrate that can provide 10% tensile strain in the [111] direction will be valid to generate band gap opening. On the other hand, based on my calculation,

when inducing compressive strain on silicene, the conductivity will increase dramatically; this can be very good sensor materials. Due to the promising properties of silicene and its ramifications, future work will be not focusing on electronics, but thermal and optical applications.

Reference

[1] L. Liao, Y. Lin, M. Bao, R. Cheng, J. Bai, Y. Liu, Y. Qu, K. L. Wang, Y. Huang and X. Duan. High-speed graphene transistors with a self-aligned nanowire gate. *Nature* 467(7313), pp. 305-308. 2010. . DOI: 10.1038/nature09405.

[2] Z. Hou and M. Yee. Electronic and Transport Properties of Graphene Nanoribbons 2007.

[3] S. MOURAS, A. HAMWI, D. DJURADO and J. COUSSEINS. Synthesis of 1st stage graphite-intercalation compounds with fluorides. *Revue De Chimie Minerale 24(5)*, pp. 572-582. 1987.

[4]K. S. Novoselov, A. K. Geim, S. V. Morozov, D. Jiang, Y. Zhang, S. V. Dubonos, I. V. Grigorieva, A. A. Firsov.. Electric Field Effect in Atomically Thin Carbon Films. *Science* 306 (5696): 666–669. doi:10.1126/science.1102896. 2004

[5] A. K. Geim and K. S. Novoselov. The rise of graphene. *Nature Materials 6(3)*, pp. 183-191. 2007.

[6] R. Qin, C. Wang, W. Zhu and Y. Zhang. First-principles calculations of mechanical and electronic properties of silicene under strain. *Aip Advances 2(2)*, pp. 022159. 2012.

[7] D. C. Elias, R. V. Gorbachev, A. S. Mayorov, S. V. Morozov, A. A. Zhukov, P. Blake, L. A. Ponomarenko, I. V. Grigorieva, K. S. Novoselov, F. Guinea, and A. K. Geim, Dirac Cones Reshaped by Interaction Effects in Suspended Graphene, *Nat. Phys.* 7, 701 (2011).

[8] X. Xu, L. F. C. Pereira, Y. Wang, J. Wu, K. Zhang, X. Zhao, S. Bae, Cong Tinh Bui, R. Xie, J. T. L. Thong, B. H. Hong, K. P. Loh, D. Donadio, B. Li and B.

Oezyilmaz. Length-dependent thermal conductivity in suspended single-layer graphene. *Nature Communications* 5pp. 3689. 2014. . DOI: 10.1038/ncomms4689.

[9] C. Lee, X. Wei, J. W. Kysar and J. Hone. Measurement of the elastic properties and intrinsic strength of monolayer graphene. *Science* 321(5887), pp. 385-388. 2008. . DOI: 10.1126/science.1157996.

[10] J. Guettinger, F. Molitor, C. Stampfer, S. Schnez, A. Jacobsen, S. Droescher, T. Ihn and K. Ensslin. Transport through graphene quantum dots. *Reports on Progress in Physics 75(12),* pp. 126502. 2012.

[11] K. Takeda and K. Shiraishi. Theoretical possibility of stage corrugation in si and ge analogs of graphite. *Physical Review B 50(20),* pp. 14916-14922. 1994.

[12] Guzmán-Verri, G. G., & Lew Yan Voon, L. C. (2007). Electronic structure of silicon-based nanostructures. *Physical Review B 76,* 075131-1 - 075131-10.

[13] S. Huang, W. Kang and L. Yang. Electronic structure and quasiparticle bandgap of silicene structures. *Appl. Phys. Lett. 102(13),* pp. 133106. 2013.

[14] R. Ansari, S. Rouhi and S. Ajori. Elastic properties and large deformation of two-dimensional silicene nanosheets using molecular dynamics. *Superlattices and Microstructures 65*pp. 64-70. 2014.

[15] L. Meng, Y. Wang, L. Zhang, S. Du, R. Wu, L. Li, Y. Zhang, G. Li, H. Zhou, W. A. Hofer and H. Gao. Buckled silicene formation on ir(111). *Nano Letters 13(2),* pp. 685-690. 2013.

[16] B. Aufray, A. Kara, S. Vizzini, H. Oughaddou, C. Leandri, B. Ealet and G. Le Lay. Graphene-like silicon nanoribbons on ag(110): A possible formation of silicene. *Appl. Phys. Lett. 96(18),* pp. 183102. 2010. . DOI: 10.1063/1.3419932.

[17] P. Vogt, P. De Padova, C. Quaresima, J. Avila, E. Frantzeskakis, M. C. Asensio, A. Resta, B. Ealet and G. Le Lay. Silicene: Compelling experimental evidence for graphenelike two-dimensional silicon. *Phys. Rev. Lett. 108(15),* pp. 155501. 2012.

[18] Ni, Zeyuan; Liu, Qihang; Tang, Kechao; Zheng, Jiaxin; Zhou, Jing; Qin, Rui;

Gao, Zhengxiang; Yu, Dapeng; Lu, Jing. Tunable Bandgap in Silicene and Germanene

Nano Letters, vol. 12, issue 1, pp. 113-118

[19] Voon, L. C. Lew Yan; Lopez-Bezanilla, A.; Wang, J.; Zhang, Y.; Willatzen, M. Effective Hamiltonians for phosphorene and silicene. New Journal of Physics, Volume 17, Issue 2, article id. 025004 (2015).

[20] Q. Pei, Z. Sha, Y. Zhang and Y. Zhang. Effects of temperature and strain rate on the mechanical properties of silicene. *J. Appl. Phys. 115(2),* pp. 023519. 2014.

[21] K. F. Mak, C. Lee, J. Hone, J. Shan and T. F. Heinz. Atomically thin MoS2: A new direct-gap semiconductor. *Phys. Rev. Lett. 105(13),* pp. 136805. 2010.

[22] B. Radisavljevic, A. Radenovic, J. Brivio, V. Giacometti and A. Kis. Single-layer MoS2 transistors. *Nature Nanotechnology 6(3),* pp. 147-150. 2011.

[23] M.E. Dávila et al., Comparative structural and electronic studies of hydrogen interaction with isolated versus ordered silicon nanoribbons grown on Ag(110), *Nanotechnology*., vol. 23, no. 385703, 2012.

[24] L.C.L.Y. Voon, E. Sandberg, R.S. Aga, and A.A. Farajian, Hydrogen compounds of group-IV nanosheets, *Appl. Phys. Lett*., vol. 97, no. 163114, 2010.

[25] N. Gao, W.T. Zheng, Q. Jiang, Density functional theory calculations for two-dimensional silicene with halogen functionalization, *Phys. Chem. Chem. Phys*., vol. 14, pp. 257-261, 2012.

[26] A. Kara, H. Enriquez, A.P. Seitsonen, and L.C. Lew, A review on silicene - New candidate for electronics, *Surf. Sci. Rep*., vol. 67, pp. 1-18, 2012.

[27] S. Cahangirov, M. Topsakal, E. Akturk, H. Sahin, and S. Ciraci, Two- and One-Dimensional Honeycomb Structures of Silicon and Germanium, *Phys. Rev. Lett*., vol. 102， no. 236804, 2009.

[28] Y. Ding, and J. Ni, Electronic structures of silicon nanoribbons, *Appl. Phys. Lett*., vol. 95, no. 083115, 2009.

[29] X. Lin, and J. Ni, Much stronger binding of metal adatoms to silicene than to graphene: A first-principles study, *Phys. Rev. B,* vol. 86, no. 075440, 2014.

[30] J. Sivek, H. Sahin, B. Partoens, and F.M. Peeters, Adsorption and absorption of boron, nitrogen, aluminum, and phosphorus on silicene: Stability and electronic and phonon properties, *Phys. Rev. B*, vol. 87, no. 085444, 2013.

[31] H. Sahin, and F.M. Peeters, Adsorption of alkali, alkaline-earth, and 3d transition metal atoms on silicone, *Phys. Rev. B*, vol. 87, no. 085423, 2013.

[32] R. Friedlein, A. Fleurence, J.T. Sadowski, and Y. Yamada-Takamura, Tuning of silicene-substrate interactions with potassium adsorption, *Appl. Phys. Lett*., vol. 102, no. 221603, 2013.

[33] H. Sahin, J. Sivek, S. Li, B. Partoens, and F.M. Peeters, Stone-Wales defects in silicene: Formation, stability, and reactivity of defect sites, *Phys. Rev. B*, vol. 88, no. 045434, 2013.

[34] J. Gao, J. Zhang, H. Liu, Q. Zhang, and J. Zhao, Structures, mobilities, electronic and magnetic properties of point defects in silicone, *Nanoscale*., vol. 5, pp. 9785-9792, 2013.

[35] Z. Ni et al., Tunable Bandgap in Silicene and Germanene, *Nano Lett.*, vol. 12, pp. 113-118, 2012.

[36] N.D. Drummond, V. Zólyomi, and V.I. Fal'ko, Electrically tunable band gap in silicone, *Phys. Rev. B*, vol. 85, no. 075423, 2012.

[37] E. Motohiko, A topological insulator and helical zero mode in silicene under an inhomogeneous electric field, *New J. Phys*., vol. 14, no. 033003, 2012.

[38] W.-F. Tsai, C.-Y. Huang, T.-R. Chang, H. Lin, H.-T. Jeng, and A. Bansil, Gated silicene as a tunable source of nearly 100% spin-polarized electrons, *Nat. Commun*., vol. 4, no. 1500, 2013.

[39] M. R. Tchalala, H. Enriquez, A. J. mayne, A. kara, S. Roth, M. G. Silly, A. Bendounan, F. Sirotti, T. Greber, B. Aufray, G. Dujardin, M. A. Ali, and H.

Oughaddou, Formation of one-dimensional self-assembled silicon nanoribbons on Au(110)-(2 x 1), *Appl. Phys. Lett*., vol. 102, no. 083107, 2013.

[40] H. H. Hall, J. Bardeen and G. L. Pearson. The effects of pressure and temperature on the resistance of P-N junctions in germanium. *Physical Review* 84(1), pp. 129-132. 1951. . DOI: 10.1103/PhysRev.84.129.

[41] C. S. Smith. Piezoresistance effect in germanium and silicon. *Physical Review* 94(1), pp. 42-49. 1954. . DOI: 10.1103/PhysRev.94.42.

[42] J. Welser, J. L. Hoyt and J. F. Gibbons. NMOS and PMOS transistors fabricated in strained silicon/relaxed silicon-germanium structures. Presented at Electron Devices Meeting, 1992. IEDM '92. *Technical Digest*., International. 1992, . DOI: 10.1109/IEDM.1992.307527.

[43] Y. Sun, S. E. Thompson and T. Nishida. Physics of strain effects in semiconductors and metal-oxide-semiconductor field-effect transistors. *J. Appl. Phys.* 101(10), pp. 104503. 2007. . DOI: 10.1063/1.2730561.

[44] J. L. Hoyt, H. M. Nayfeh, S. Eguchi, I. Aberg, G. Xia, T. Drake, E. A. Fitzgerald and D. A. Antoniadis. *Strained Silicon MOSFET Technology* 2002.

[45]Y. Zhang, R. Tsu. Binding Graphene Sheets Together Using Silicon: Graphene/Silicon Superlattice. *Nanoscale Research* Letters, 5:805-808

[46] B. Lalmi, H. Oughaddou, H. Enriquez, A. Kara, S. Vizzini, B. Ealet and B. Aufray. Epitaxial growth of a silicene sheet. *Appl. Phys. Lett. 97(22),* pp. 223109. 2010.

[47] S. Cahangirov, M. Topsakal, E. Akturk, H. Sahin and S. Ciraci. Two- and one-dimensional honeycomb structures of silicon and germanium. *Phys. Rev. Lett. 102(23),* pp. 236804. 2009.

[48] N. D. Drummond, V. Zolyomi and V. I. Fal'ko. Electrically tunable band gap in silicene. *Physical Review B 85(7),* pp. 075423. 2012.

[49] Q. Peng, X. Wen and S. De. Mechanical stabilities of silicene. *Rsc Advances* 3(33), pp. 13772-13781. 2013. . DOI: 10.1039/c3ra41347k.

[50] N. B. Le, Tran Doan Huan and L. M. Woods. Tunable spin-dependent properties of zigzag silicene nanoribbons. *Physical Review Applied* 1(5), pp. 054002. 2014. . DOI: 10.1103/PhysRevApplied.1.054002.

[51] G. Liu, M.S.Wu, C.Y. Ouyang, B. Xu, *EPL (Europhysics Letters)* 99(1), 17010 (2012).

[52] B. Wang, J. Wu, X. Gu, H. Yin, Y. Wei, R. Yang, M. Dresselhaus, Applied *Physics Letters* 104(8), 081902 (2014). DOI. http://dx.doi.org/10.1063/1.4866415.

[53] T. P. Kaloni, Y. C. Cheng, U. Schwingenschl¨ogl, Hole doped Dirac states in silicene by biaxial tensile strainJ. App. *Phys.* 113, 104305 (2013)

[54] C. Yang, Z. Yu, P. Lu, Y. Liu, H. Ye, T. Gao, *Computational Materials Science* 95(0), 420 (2014). DOI http://dx.doi.org/10.1016/j.commatsci.2014.07.046.

[55] S. Kokott, P. Pflugradt, L. Matthes and F. Bechstedt. Nonmetallic substrates for growth of silicene: An ab initio prediction. *Journal of Physics-Condensed Matter 26(18)*, pp. 185002. 2014.

[56] Y. Ding and Y. Wang. Electronic structures of silicene/GaS heterosheets. *Appl. Phys. Lett. 103(4)*, pp. 043114. 2013.

[57] A. Bhattacharya, S. Bhattacharya and G. P. Das. Exploring semiconductor substrates for silicene epitaxy. *Appl. Phys. Lett. 103(12)*, pp. 123113. 2013.

[58] P. Lawaetz. Stability of wurtzite structure. *Physical Review B* 5(10), pp. 4039-&. 1972. . DOI: 10.1103/PhysRevB.5.4039.

[59] M. I. McMahon and R. J. Nelmes. Observation of a wurtzite form of gallium arsenide. *Phys. Rev. Lett*. 95(21), pp. 215505. 2005. . DOI: 10.1103/PhysRevLett.95.215505.